Chapter 7

# Actinide Pincer Chemistry: A New Frontier

**Connor S. MacNeil, Tara K.K. Dickie and Paul G. Hayes**
*University of Lethbridge, Lethbridge, AB, Canada*

**Chapter Outline**

## 7.1 INTRODUCTION

Chemistry with actinide metals has historically been underdeveloped due to the inherent difficulties in handling molecular actinide complexes. Actinide chemistry is generally only practiced with thorium and uranium for reasons of cost and availability, as well as radioactivity. While all the actinide elements are radioactive, thorium and uranium have extremely long half-lives compared to most other metals in the actinide series. Thorium-232 is an $\alpha$-emitter with $t_{1/2} >$ 14 billion years. Depleted uranium is primarily U-238, which also emits an $\alpha$-particle when it decays and has a half-life of more than 4 billion years. For these reasons, uranium and thorium are generally considered weakly radioactive [1,2]. Despite the associated complications, actinide chemistry is of great fundamental interest, and has thus blossomed into a rapidly emerging subfield of both inorganic and organometallic chemistry.

The actinide metals are similar to the lanthanides in size, but have access to a greater number of oxidation states, a trait more commonly shared with transition metals. The actinide elements are also recognized for their ability to form complexes with high coordination numbers ($>6$) which can lead to unique chemical transformations. Such reactivity is also often attributed to the large, diffuse *f*-orbitals which participate much more in covalent bonding than their lanthanide counterparts [3,4]. Notably, computational investigations have shown that the actinide 5*f* orbitals provide access to chemical transformations which are not possible with transition metals because of their ability to hybridize and stabilize transition states that would normally be inaccessible [5,6]. In June of 2017, a 60-year-old debate sparked by Glenn Seaborg on the covalent nature of the actinide−chlorine bond [7] may have been resolved experimentally [8]. Compelling evidence for 5*f*−3*p* orbital mixing in $AmCl_6^{3-}$ was obtained using X-ray absorption spectroscopy (XAS). Covalency in actinide−ligand bonding is also relevant to nuclear waste management (see Section 7.3.1), where the topic is hotly debated.

Although uranium and thorium are both actinide metals, each display markedly different reactivity. Thorium can generally only access the $4+$ oxidation state, while uranium complexes in the $3+$ to $6+$ oxidation states are commonly reported ($3+$ and $5+$ tend to be the most reactive) [1]. The enhanced reactivity of An(III) ions comes at a cost; the negative reduction potential ($E^{\Theta} = -0.6$ V (U), $-3.7$ V (Th) for the $M^{IV/III}$ redox couple in $MX_6$ ions) [9] discourages redox cycles needed in certain catalytic reactions. Nevertheless, the greater range of readily available

oxidation states avails a wide realm of potential chemistry, but it can also lead to additional decomposition pathways, particularly for species in solution. Tetravalent uranium, the most common oxidation state for that metal, is also paramagnetic, which can present challenges regarding characterization via NMR (nuclear magnetic resonance) spectroscopy, such as line broadening, loss of coupling, and huge chemical shift ranges [10].

Organoactinide chemistry traces its roots to heteroleptic $\pi$-complexes (e.g., $(Cp^*/Cp)_2AnX$, $Cp^* = C_5Me_5{}^-$; $Cp = C_5H_5{}^-$; $X = I$, Cl), much in the same way organotransition metal chemistry became popularized by discrete single-metal $\pi$-complexes and the metallocene class, $Cp_2M$ ($M$ = transition metal) [11]. Early publications highlighted the successful pairing of carbocyclic ligands and actinide metals; Marks [12−14], Evans [8,15−17], Ephritikhine [18−21], and others have contributed pioneering work in this respect (Chart 7.1). Notably, as the structural diversity of available ancillary ligands has increased considerably over the past several decades, exciting and unprecedented reaction chemistry and catalysis involving $d$-block, lanthanide, and actinide metals has been reported at a continuously accelerating rate. In the most recent annual survey of the organometallic chemistry of lanthanides and actinides, Edelmann remarks that "approximately 20% of the papers published in 2015 were in the area of organoactinide chemistry" [4].
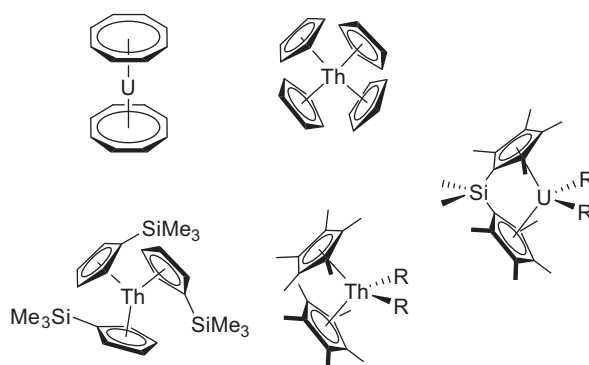


**CHART 7.1**   Examples of organoactinide complexes supported by carbocyclic ligands.

Hybrid ligands that incorporate both soft and hard donors can engender reactivity not available to the metallocenes. The development of meridionally coordinating pincer ligands has been a watershed moment in this respect, and has contributed to the advancement of knowledge insofar that entirely new fields have evolved. For example, David Milstein has published a substantial body of work that enhances our understanding of how pincer ligands and metals cooperate in chemical transformations, particularly with respect to the lofty goal of catalytically functionalizing unactivated hydrocarbons and simple diatomics ($N_2$, CO, CN) [22]. Redox-active pincer ligands capable of multielectron transformations (Section 7.3.5) have conferred noble metal reactivity to first-row d-block elements (Fe, Co, Ni, Mn). Since the first edition of this text was published [23], the use of pincer ligands has continued to grow. This popularity has increased the breadth of pincer complexes to include rare earth [24], and more recently, actinide metals, the subject of this review.

It is important to outline the criteria used to define a pincer ligand. Many distinctions have been made, all of which recognize that the ligand's three donor sites occupy a shared meridional plane, forming five- or six-membered metalloheterocycles (Fig. 7.1). Of course, occasional deviations from this prototypical definition warrant inclusion; in Section 7.3.3.2 a dianionic pincer carbene ligand defined by four-membered metalloheterocycles is discussed.

Although 40 years have passed since polyfunctional pincer ligands were introduced to transition metals, actinide pincer chemistry has only recently established its footing. As this rapidly expanding field matures, we are of the opinion
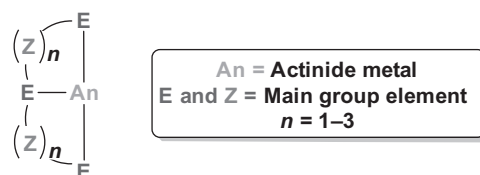


**FIGURE 7.1**   General definition of an actinide pincer complex.

that a sufficient body of work has accumulated, such that a comprehensive review is justified. As a whole, actinide chemistry continues to be dominated by sterically demanding carbocyclic ligand sets, a consequence of large ionic radii and preference for high coordination number. Herein lies the main challenge of actinide chemistry, the delicate balance between stabilizing the reactive metals without rendering them inert. To this end, rational ligand design has been a huge boon to the area of actinide chemistry. The pincer-based chemistry outlined herein can be described as a synthetic renaissance in actinide chemistry and represents a second phase of the post-metallocene era.

## 7.2 GENERAL SYNTHETIC STRATEGIES FOR PREPARING ACTINIDE PINCER COMPLEXES

The comparatively slow progression of actinide chemistry is due in part to the geopolitical constraints placed on the acquisition and transport of radiotoxic metals. A compounding effect of this reality is that viable actinide starting materials are less common than for rare earth and transition metals, which are not typically under such strict regulations. Despite these challenges, actinide halide complexes have become available by operationally simple protocols, and a handful of reports outlining the preparation of valuable uranium and thorium halide solvento adducts ($UBr_3(THF)_4$ [25], $UI_3(THF)_4$ [25], $UI_3(DME)_2$ [25], $UI_3(py)_4$ [25], $UI_4(OEt_2)_2$ [26], $UI_4(NCMe)_4$ [27], $UI_4(NCPh)_4$ [28], $ThCl_4(THF)_{3.5}$ [29], $ThBr_4(THF)_4$ [30], $ThBr_4(py)_4$ [30], $ThBr_4(NCMe)_4$ [30], $ThI_4(THF)_4$ [31], $ThCl_4(1,4\text{-dioxane})_2$ [29], $ThCl_4(DME)_2$ [29], $ThI_4(DME)_2$ [31]; DME = 1,2-dimethoxyethane, py = pyridine) have been disclosed. The stability of these starting materials allows for reliable preparation and handling, which is crucial for any synthetic campaign. Given that actinide complexes often suffer from thermal instability, it should come as no surprise that cases of decomposition have been observed in solvated actinide species, and thus, such reactivity must be kept in mind. For example, $ThI_4(DME)_2$ is robust whereas $ThI_4(THF)_4$ undergoes ring opening of THF to afford $ThI_3[O(CH_2)_4I](THF)_3$ [31]. Furthermore, $UI_3(1,4\text{-dioxane})$ demonstrates substantial thermal stability and is resistant to deleterious pathways that plague the analogous THF adducts. While uranium and thorium are the only actinide metals for which pincer complexes have been reported, neptunium and plutonium starting materials are available as solvated trivalent iodide complexes $NpI_3(THF)_4$ [25], $PuI_3(THF)_4$ [25], $PuI_3(py)_4$ [25], $PuI_3(Et_2O)_x$ [32] and, and more recently, as tetravalent chloride species, $NpCl_4(DME)_2$ and $PuCl_4(DME)_2$ [33]. From the availability of these complexes, significant potential for pincer chemistry with transuranic elements exists. Given that salt metathesis protocols represent the predominant entry point for pincer-supported actinide chemistry, any improvement upon the synthesis of actinide halides is of noteworthy.

Alkane elimination has been used to generate pincer complexes from proteo ligands and solvated trisalkyl rare earth compounds [24]. Examples where favorable alkane elimination has resulted in pincer complex formation are not as common for the actinides but are discussed where relevant. A glaring absence in the availability of stable organoactinide reagents capable of alkane elimination pathways has undoubtedly slowed progress in this area. A 2015 report on the improved and new syntheses of various homoleptic U(IV) benzyl derivatives by Bart and coworkers could represent a turning point in the practicality of using alkane elimination strategies to generate well-defined actinide pincer complexes (Scheme 7.1) [12,34]. Arnold and coworkers [35] recently added to this discussion by providing details on the formation of the homoleptic U(III) aryl complex $U[2,6-(4-^tBuC_6H_4)_2C_6H_3]_3$, which contains reactive U−C bonds, and facilitates the double insertion of $^iPrN = C = N^iPr$. Thus, there is clearly growing potential for alkane elimination routes as diverse avenues into actinide pincer chemistry. Finally, amine elimination methods, though even less common, have been explored using $U(NEt_2)_4$ [36]. The availability of $An(N(SiMe_3))_3$ (An = U, Np, Pu) [25,32] will likely also prove useful for generating An(III) pincer complexes bearing amido functionalities.
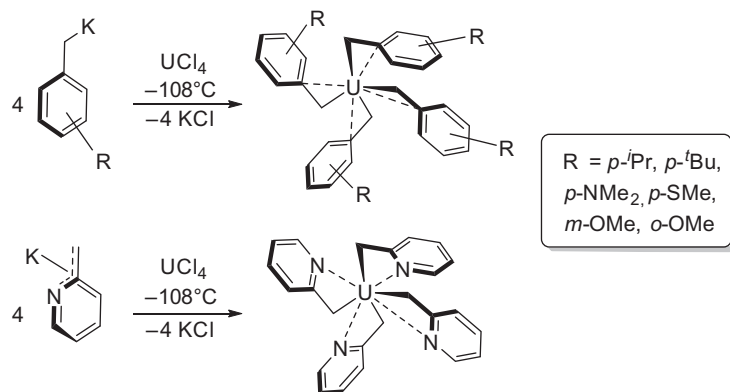


**SCHEME 7.1** Synthesis of tetrabenzyluranium derivatives.

## 7.3  SYNTHESIS, STRUCTURE, AND STOICHIOMETRIC REACTIVITY OF ACTINIDE PINCER COMPLEXES

### 7.3.1  Neutral Ligands

Perhaps the most cited motivation for combining neutral pincer ligands with actinides has been the sequestration of nuclear waste products, specifically to affect the separation of actinides from lanthanides [20,21,37,38]. Pincer ligands based on aromatic *N*-heterocycles have been the focus of much of these efforts. In the final stages of fuel reprocessing, minor actinides (americium and curium) are packaged with fission products in vitrified nuclear waste. After the decay of short-lived isotopes, the contributions by minor actinides to bulk waste radioactivity become significant. Because of safety, practical, and legislative reasons, research into actinide separation is uncommon. In response to these concerns, trivalent uranium, which can be handled with relative ease, has served as a representative actinide for studying sequestration in aqueous and organic An(III)/Ln(III) mixtures.



CHART 7.2   Neutral *NNN* pincer ligands based on *N*-heterocycles.

terpy

$^R$btp
R = Me, $^n$Pr

2,4,6-tris(2-pyridyl)-1,3,5-triazine

pK$_a$:
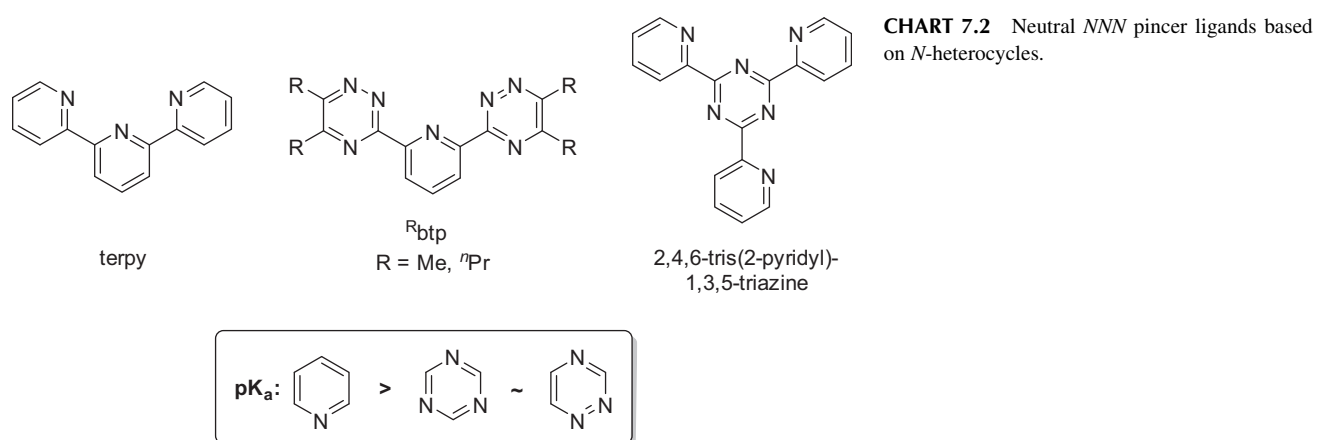
In a series of publications, competition experiments were performed to quantify the separation of uranium from metals in the lanthanide series [Ce, Nd, La] using neutral *NNN* pincer ligands (Chart 7.2) [20,21,37,38]. Of the ligands that exhibit affinity for trivalent uranium, derivatives of btp (2,6-bis(5,6-dialkyl-1,2,4-triazin-3-yl)pyridines) have proven to be the most effective [37]. In a $^1$H NMR competition experiment, a mixture of UI$_3$ and CeI$_3$ was titrated with three molar equivalents of a btp ligand (R = Me) [37]. Differential complexation was authenticated by comparing the spectroscopic data to complexes synthesized independently. Strikingly, only the triligand complex [U($^{Me}$btp)$_3$]I$_3$, **1**, was observed (Scheme 7.2); no significant cerium complexation was detected (5%). Only through the addition of excess btp ligand were the di- and triligand complexes of cerium, [Ce($^{Me}$btp)$_2$]I$_3$ and [Ce($^{Me}$btp)$_3$]I$_3$, observed. Such high levels of selectivity for uranium over cerium by btp encouraged research into further rational design of neutral *N*-heterocyclic ligands for separation chemistry [20,21,39], which Ephritikhine and coworkers have largely pioneered. Notably, it was discovered that the 2,2′:6′,2″-terpyridine (terpy) ligand exhibits only modest actinide(III) affinity compared to btp systems [19]. The heightened covalency of the U−N bonds in btp complexes, and hence increased U(III) affinity by btp ligands, has been attributed to the decreased basicity of triazines (pK$_a$ of conjugate acid < 0), compared to pyridine (pK$_a$ of conjugate acid = 5.2).



SCHEME 7.2   Selective complexation of U(III) (dark spheres) over Ce(III) (light spheres) by the neutral $^{Me}$btp ligand.

$^{Me}$btp

○ = UI$_3$   ○ = CeI$_3$

[U($^{Me}$btp)$_3$]I$_3$

**1**
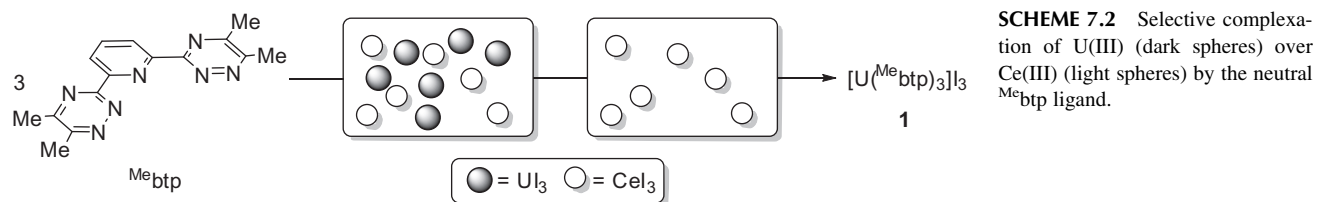
Neutral ligands based on aromatic *N*-donors have been successfully complexed to uranium iodides [19], triflates [20], and more recently, metallocenes [18]. In the context of organoactinide chemistry, the combination of neutral terpy ligands with actinocenes is highly relevant. For example, addition of terpy to the tetravalent complex [Cp*$_2$U(NCMe)$_5$] [BPh$_4$]$_2$ in THF afforded the linear actinocene species [(terpy)UCp*$_2$(NCMe)$_2$][BPh$_4$]$_2$, **2** (Scheme 7.3) [18]. While the neutral terpy ligand provided stable complexes in both coordinating solvent and the solid state, ligand-based reduction using sodium amalgam generated a radical anion that exhibited redox activity, complete details of which are discussed in depth in Section 7.3.5.3.
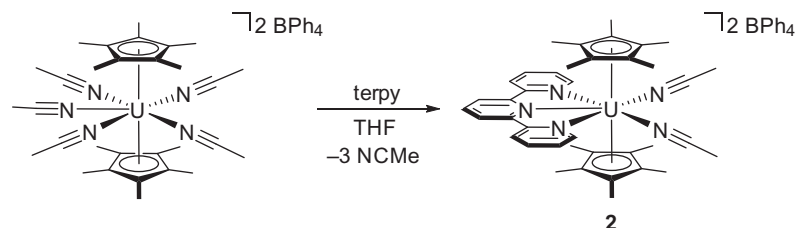


**SCHEME 7.3** Reaction of a terpy ligand with the cationic uranocene solvate [Cp*$_2$U(NCMe)$_5$][BPh$_4$]$_2$.

## 7.3.2 Monoanionic Ligands

### 7.3.2.1 PNP *Ligands*

In a seminal contribution by Kiplinger and coworkers, Ozerov's monoanionic PNP ligand (PNP = [2-P(CHMe$_2$)$_2$-4-MeC$_6$H$_3$]$_2$N$^-$) was shown to support uranium iodide, chloride, and significantly, uranyl complexes [40,41]. Recognizing that the combination of Cp*$_2$UI(THF) and sodium amalgam provided a U(II) synthetic equivalent capable of 4-electron reduction chemistry [40,42], the diligand complex [PNP]$_2$UI, **3**, was targeted for the analogous chemistry by Kiplinger (Scheme 7.4). In this study, direct and systematic comparisons between uranium complexes supported by pincer and cyclopentadienide ligands were performed for the first time. The pincer complex [PNP]$_2$UI was shown to promote reaction chemistry not otherwise available using a Cp-based ligand set, validating the actinide pincer combination [40,41].
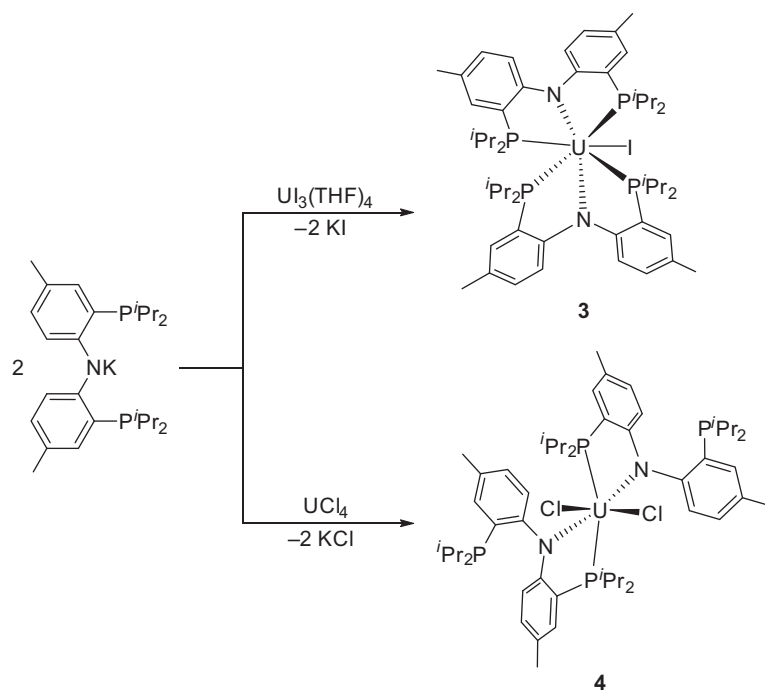


**SCHEME 7.4** Synthesis of mono- and bis(PNP) uranium complexes **3** and **4**.

A drawback associated with actinocene reactivity, namely the ejection of $(C_5Me_5)_2$ upon oxidation, prompted further study of bis(PNP) complexes of uranium, which boast greater steric protection of, and electron donation to, the electropositive metal. To this end, the potassium salt of the PNP ligand, K[PNP], was prepared by straightforward deprotonation of the proteo ligand with potassium bis(trimethylsilyl)amide to afford a yellow solid in 92% yield. Salt metathesis provided access to the requisite uranium(III) and uranium(IV) halide complexes [PNP]$_2$UI, **3**, and [PNP]$_2$UCl$_2$, **4** Scheme 7.4. Alternatively, when the ligand attachment protocol was conducted in the presence of external Lewis base, monoligand trihalide complexes [PNP]UX$_3$(L)$_{1-2}$ (X = Cl, I; L = (O)PMe$_3$, **5-OPMe$_3$**; (O)PPh$_3$, **6-OPPh$_3$**; THF, **7-THF**) were produced exclusively (Scheme 7.5). Complex **7-THF** showed no indication of competitive THF ring opening, a process often invoked by rare earth and actinide complexes (*vide supra*) [41].
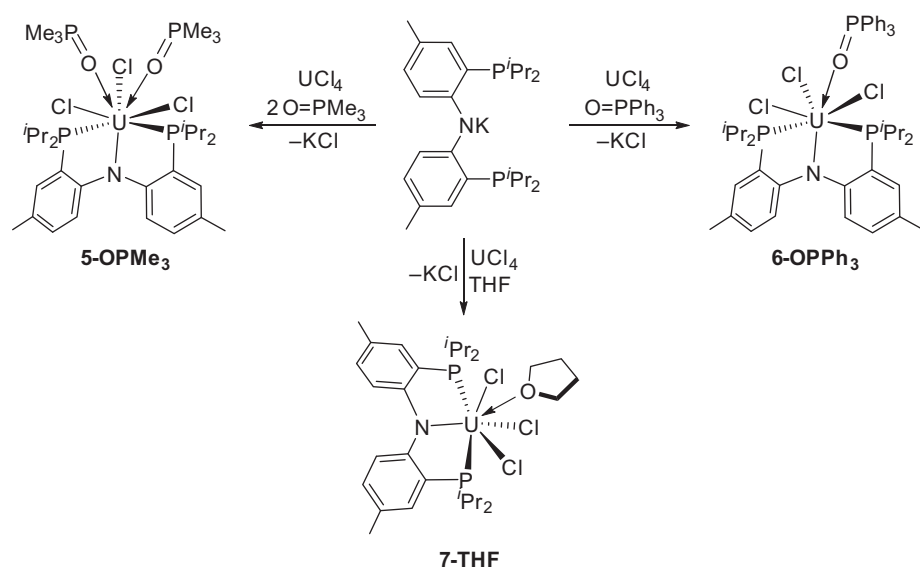


**SCHEME 7.5**  Synthesis of mono(PNP) uranium complexes using external Lewis bases.

While PNP is more sterically demanding than Cp*, dissociation of the labile phosphine donors can increase access to the metal center (Fig. 7.2), as suggested by the structure of complex **4**. Management of the steric environment around a reactive metal by variable coordination of a hemilabile ligand in a synthetic or catalytic cycle is a hallmark of metal−ligand cooperation and presents an opportunity for pincer ligands [22]. In complex **3**, where the actinide is bound to a single halide ligand, a $\kappa^3$-($P,N,P$) coordination mode was observed in both solution and solid state. In complex **4**, however, the $\kappa^2$-($P,N$) motif prevails, with two chloride ligands completing the coordination sphere of the tetravalent uranium center. The variable coordination of the PNP system can easily be monitored by $^{31}$P NMR spectroscopy, as bound and free phosphines exhibit diagnostic chemical shifts ($\delta$ 1401.1 and 50.3, respectively, for [PNP]$_2$UCl$_2$, **4**) [40,41].

In related work by the same group, both $\kappa^3$-($P,N,P$) and $\kappa^2$-($P,N$) coordination modes were observed in the remarkable uranyl complex, [PNP]$_2$U(O)$_2$, **8**. Starting from trivalent [PNP]$_2$UI, **3**, the uranyl complex was generated by
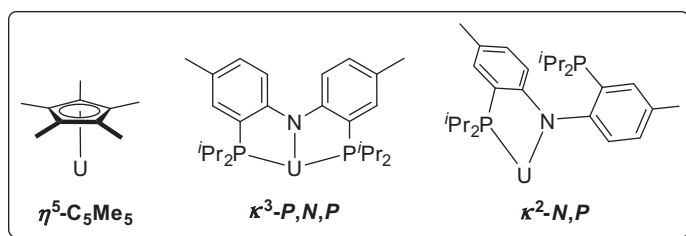


**FIGURE 7.2**   Common bonding modes for Cp* and PNP ligands.

chemical oxidation using 2 equivalents of pyridine-*N*-oxide and $KC_8$ (Scheme 7.6) [40]. Notably, this species represents the first example of a uranyl phosphine complex. Given that the pairing of soft ligands with the hard $[UO_2]^{2+}$ fragment is generally thought of as disfavored, this result illustrates the flexibility of the PNP ligand in accommodating the highest oxidation state of uranium (6+). Chemical oxidation of $Cp*_2UI(THF)$ under identical conditions gave only mixtures of uranium oxides, along with the $(C_5Me_5)_2$ dimer as the sole organic product [40]. Evidently, under these conditions the PNP pincer scaffold, likely due in part to its readily available coordinative flexibility, is better suited than $Cp*$ at supporting both low- and high-valent uranium (3+ and 6+), thus providing opportunity to harness redox chemistry in bond activation strategies.
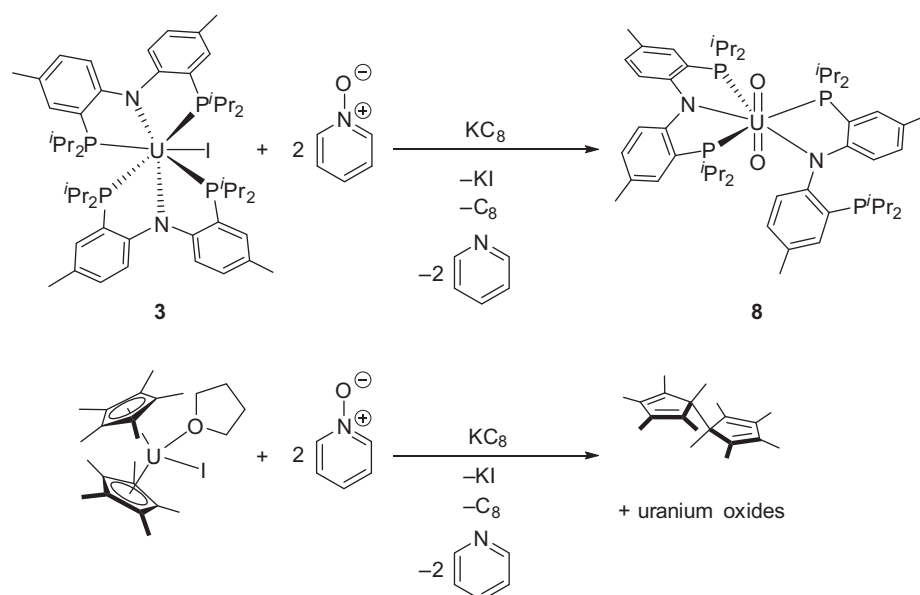


SCHEME 7.6 Comparative oxidation reactivity of uranium pincer and Cp* complexes.

To survey additional redox reactivity, $Cp*_2UI(THF)/KC_8$ and **3**/$KC_8$ were reacted with diphenyldiazomethane ($Ph_2C=N_2$) [40]. Quantitative formation of the uranium(IV) hydrazonido complex $[PNP]_2U(\eta^2\text{-}((N,N') = N-N = CPh_2)$, **9**, resulted from a 2-electron reduction of the organic substrate (Scheme 7.7). Again, the PNP ligand displayed flexible coordination in product **9**, with both $\kappa^3\text{-}(P,N,P)$ and $\kappa^2\text{-}(P,N)$ bonding modes present. The extent of reduction was more pronounced when the trivalent complex $Cp*_2UI(THF)$ was employed; 2 equivalents of the oxidant were required to complete the reaction wherein the fully oxidized U(VI) $Cp*_2U(=N-N=CPh_2)_2$ was produced [40]. These observations validate PNP as a viable framework for supporting actinide metals under oxidizing conditions, and should serve to inspire continued growth within this realm [43].
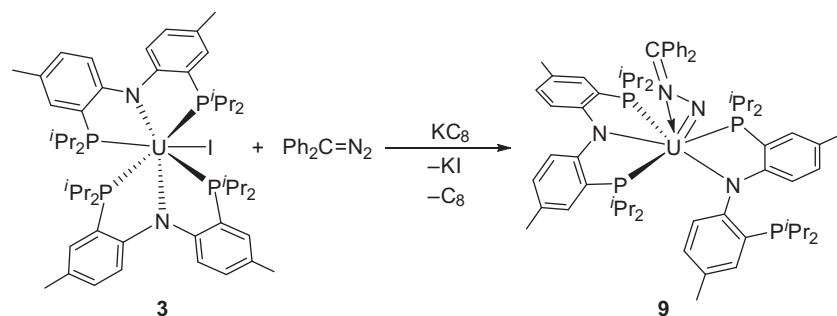


SCHEME 7.7 Partial oxidation of $[PNP]_2UI$, **3**.

### 7.3.2.2 SPS *Ligands*

Ephritikhine, Le Floch, and coworkers [44] have demonstrated that an entirely soft donor set (S,P) can also be used to stabilize uranium(IV) complexes. The unique monoanionic pincer ligand, $^{Me}$SPS [SPS = 2,6-bis(diphenylphosphinesulfide)-3,5-diphenylphosphinine] was constructed from a central $\lambda^4$-phosphinine unit bearing two phosphine sulfide ($R_3P$=S) groups. Diligand uranium complexes [$^{Me}$SPS]$_2$UX$_2$ (X = Cl, **10-Cl**; BH$_4$, **10-BH$_4$**) were generated in high yields through salt metathesis of the lithiated or potassiated ligands Li[$^{Me}$SPS], K[$^{Me}$SPS], and UX$_4$ (X = Cl, BH$_4$) (Scheme 7.8) [45].
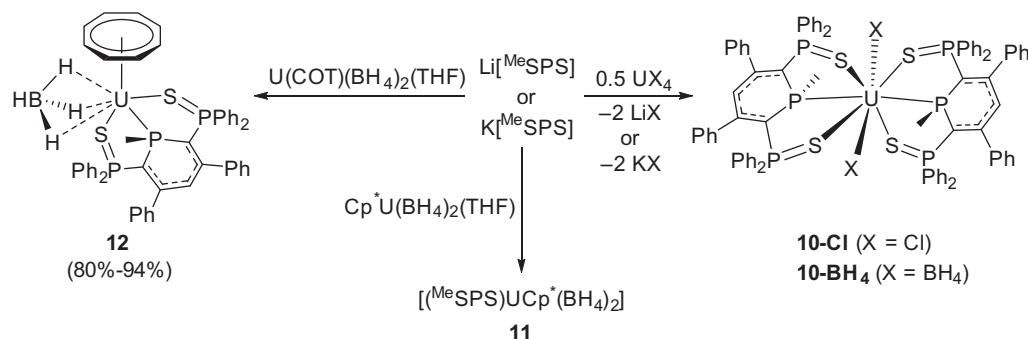


SCHEME 7.8 Synthesis of tetravalent uranium complexes supported by an SPS ligand.

Organometallic complexes were later targeted as a means to expand on this chemistry. Notably however, attempts at generating monoligand complexes with cyclopentadienide ligands were met with difficulties. Combinations of Cp$_3$UCl and Cp*$_2$UX$_2$ (X = Cl, BH$_4$) with lithiated or potassiated $^{Me}$SPS provided no evidence of complex formation, due in part to the sterically hindered nature of the organometallic reagents. Opting for trivalent Cp$_3$U(THF) only gave the sulfide-bridging complex [{Cp$_3$U}$_2$($\mu$-S)], demonstrating the ability of U(III) to reduce the ligand phosphine sulfide groups [44]. The less sterically encumbered complex Cp*U(BH$_4$)$_3$ reacted with [K(OEt$_2$)][$^{Me}$SPS] in THF, generating [$^{Me}$SPS]UCp*(BH$_4$)$_2$, **11**, in 70% yield. Likewise, U(COT)(BH$_4$)$_2$(THF) reacted with lithiated or potassiated $^{Me}$SPS, providing the expected product [$^{Me}$SPS]U(COT)(BH$_4$), **12**, in 80% and 94% yield, respectively. The stability of the $^{Me}$SPS pincer ligand in **12** contrasts the methoxide analogue $^{OMe}$SPS, which undergoes P−O bond cleavage to give a complicated mixture of products including [$^H$SPS]U(COT)(BH$_4$), **13**. Attempts were made at a more convenient synthesis of complex **13**, with addition of catalytic NaBH$_4$ to the reaction eventually giving the product in 79% yield [44] (Scheme 7.9).
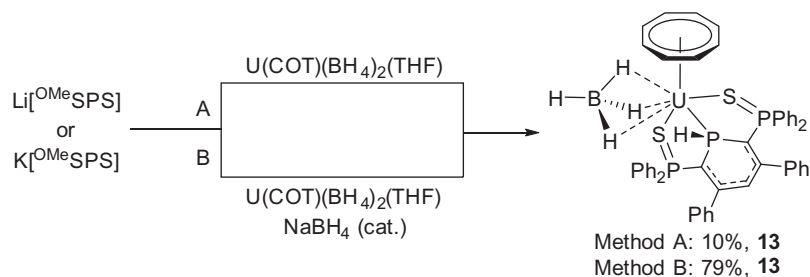


SCHEME 7.9 Alternate pathways to synthesize complex **13**.

The bonding situation in the SPS pincer ligand was the focus of computational analyses using density functional theory (DFT) [46]. It was shown that the overall 1 − charge on the SPS pincer ligand is stabilized by charge delocalization in the phosphahexadienyl (C$_5$P) ring, and by negative hyperconjugation into the antibonding P−R orbital ($\sigma$* R = Me, OMe). The latter interaction could contribute to the observed P−O bond reactivity in the formation of complex **13**, as well as P−C bond lengthening in the related $^{Me}$SPS ligand.

### 7.3.2.3 NCN Ligands

Liddle et al. [47] have conducted a series of investigations to assess the extent of covalency in actinide−carbon multiple bonds (Section 7.3.3.2). While developing pincer carbene complexes where the ligands bear a formal $2-$ charge and take the form of $[C(PPh_2NR)_2]^{2-}$ (R = 2,6-$^i$Pr$_2$C$_6$H$_3$ (Dipp), $^{Dipp}$BIPM; 2,4,6-Me$_3$C$_6$H$_2$ (Mes), $^{Mes}$BIPM; and SiMe$_3$ (TMS), $^{TMS}$BIPM), monoanionic *NCN* ligands $[HC(PPh_2NR)_2]^{1-}$ (R = Mes, H$^{Mes}$BIPM, SiMe$_3$, H$^{TMS}$BIPM), with central methanide donors, were also studied [47,48]. When the ligand salts K[H$^R$BIPM] and Na[H$^{Mes}$BIPM] were combined with UCl$_4$(THF)$_3$ or UCl$_4$ and UO$_2$Cl$_2$(THF)$_2$, respectively, salt metathesis gave methanide complexes [H$^R$BIPM]UCl$_3$(THF), (R = Mes, **14** [47], SiMe$_3$, **15** [48], Scheme 7.10) and [H$^{Mes}$BIPM]U(O)$_2$Cl(THF), **16** (Scheme 7.11). The X-ray crystal structures of **14** and **16** contain U−C bond lengths of 2.779(2) Å and 2.793(2) Å, respectively, and can be compared to the analogous species [H$^{TMS}$BIPM]UCl$_3$(THF), **15**, [2.709(4) Å], and [H$^{TMS}$BIPM]U(O)$_2$Cl(THF), **17**, [2.707(4) Å], which contain the less sterically demanding SiMe$_3$ groups on nitrogen [48−50]. The THF-free dimer of **17**, [(H$^{TMS}$BIPM)U(O)$_2$Cl]$_2$, **18**, can be generated by removal of THF from complex **17**.
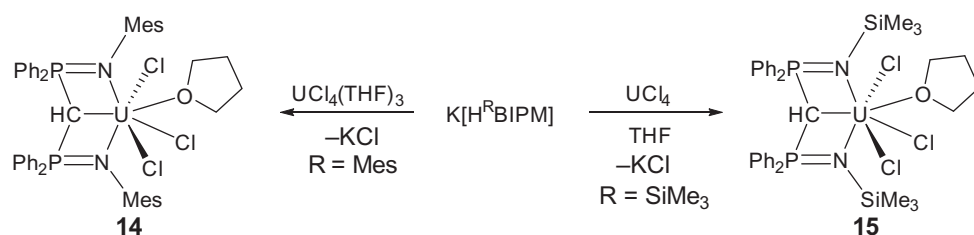


SCHEME 7.10 Synthesis of *NCN* pincer complexes **14** and **15**.
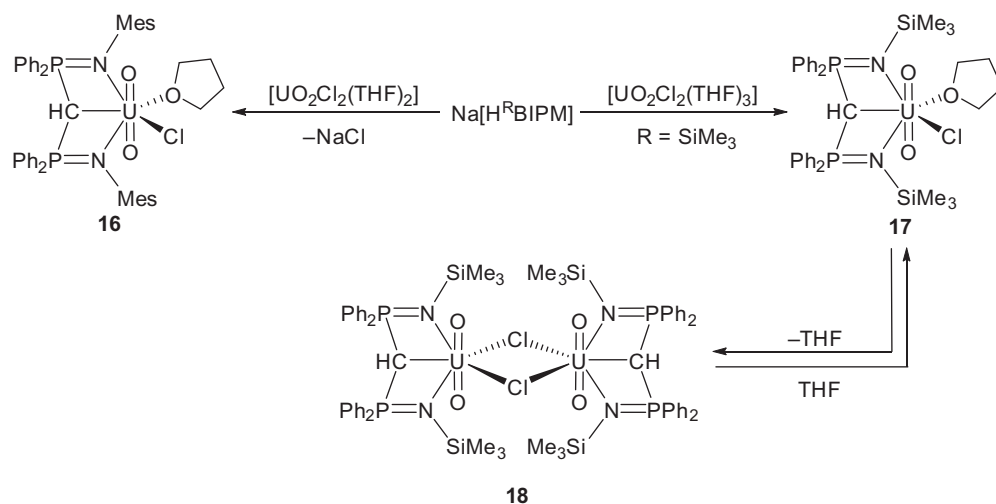


SCHEME 7.11 Synthesis of uranyl complexes **16−18**.

### 7.3.2.4 NNN Ligands

Hayes and coworkers [51−54] have been developing actinide pincer complexes based on an *NNN*-monoanionic scaffold featuring a pyrrole backbone. This advancement follows the successful use of this ligand system to support a range of rare earth and transition metals. Reaction of AnCl$_4$(DME)$_2$ (An = U, Th; DME = dimethoxyethane) with NaL (**L** = 2,5-(R$_2$P = NAr)$_2$N(C$_4$H$_2$)$^-$, R = Ph, $^i$Pr; Ar = 4-$^i$PrC$_6$H$_4$, 2,6-$^i$Pr$_2$C$_6$H$_3$) cleanly afforded the anticipated family of trichloride pincer complexes **L**UCl$_3$, **19-U**, and **L**ThCl$_3$, **20-Th**, which are thermally stable for days in solution. Chloride abstraction with [CPh$_3$][B(C$_6$F$_5$)$_4$] in Lewis basic solvent provided thorium and uranium cationic complexes [**L**UCl$_2$(THF)][B(C$_6$F$_5$)$_4$], **20-U**, and [**L**ThCl$_2$(DME)][B(C$_6$F$_5$)$_4$], **20-Th**, with THF and DME, respectively, in the vacant coordination site (Scheme 7.12) [55].
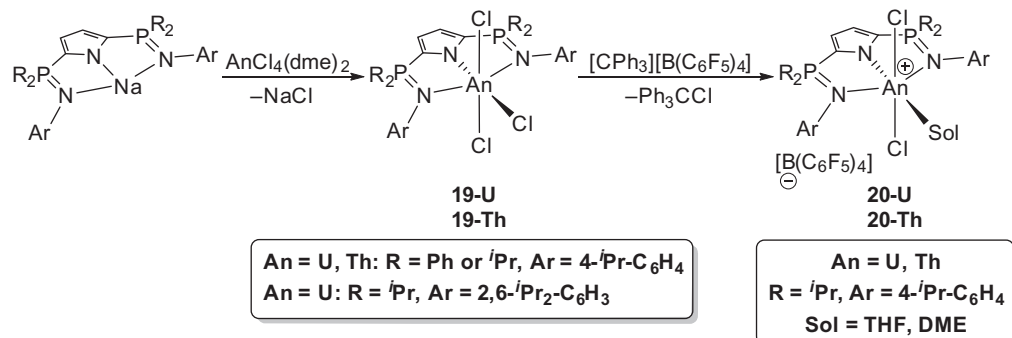
SCHEME 7.12 Synthesis of cationic actinide complexes 20-U and 20-Th.

**19-U**
**19-Th**

An = U, Th: R = Ph or $^i$Pr, Ar = 4-$^i$Pr-C$_6$H$_4$
An = U: R = $^i$Pr, Ar = 2,6-$^i$Pr$_2$-C$_6$H$_3$

**20-U**
**20-Th**

An = U, Th
R = $^i$Pr, Ar = 4-$^i$Pr-C$_6$H$_4$
Sol = THF, DME

## 7.3.3 Dianionic Ligands

### 7.3.3.1 NON/NSN Ligands

Dianionic ligands constructed about central ether donors have enabled the preparation of numerous tetravalent uranium and thorium alkyl complexes. As with monoanionic pincers (Section 7.3.2), electronic and steric tunability is an attractive feature of the dianionic *NON/NSN* classes, particularly given the pronounced effect that altering groups on the flanking amido donors (Ph, $^t$Bu, Dipp; Dipp = 2,6-$^i$Pr$_2$C$_6$H$_3$) can have upon compound stability and reactivity. For example, the Emslie group has synthesized a pincer ligand that features a modified xanthene core and two anionic amides. This ligand system has been shown to support remarkably stable organoactinide complexes. When K$_2$(DME)$_2$[XA$_2$] (XA$_2$ = 4,5-bis(2,6-diisopropylanilido)-2,7-di-*tert*-butyl-9,9-dimethylxanthene; DME = 1,2-dimethoxyethane) was combined with ThCl$_4$(DME)$_2$ in toluene, a robust dichloride [XA$_2$]ThCl$_2$(DME), **21**, which displays pentagonal bipyramidal geometry in the solid state, was isolated (Scheme 7.13) [56].
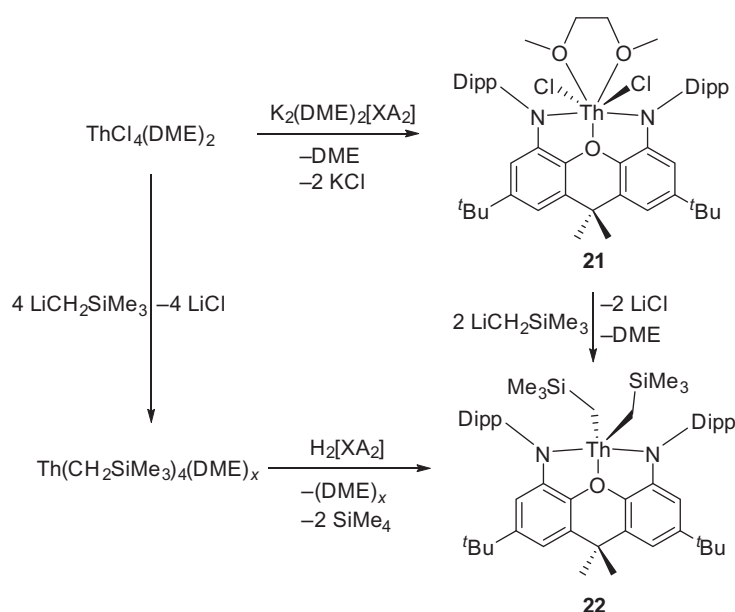


SCHEME 7.13 Synthesis of XA$_2$-supported organothorium complex **22**.

Notably, the addition of 2 equivalents of LiCH$_2$SiMe$_3$ to [XA$_2$]ThCl$_2$(DME) afforded the base- and salt-free thorium dialkyl [XA$_2$]Th(CH$_2$SiMe$_3$)$_2$, **22**. Further, complex integrity is maintained in solution at 70°C for multiple days, which is uncharacteristically stable for a non-Cp organoactinide complex. Interestingly, [XA$_2$]Th(CH$_2$SiMe$_3$)$_2$ can be synthesized independently by the reaction of ThCl$_4$(DME)$_2$ with 4 equivalents of LiCH$_2$SiMe$_3$ at low temperature for 2 h followed by addition of H$_2$[XA$_2$] at −78°C. The success of this methodology implies an alkane elimination pathway that

proceeds through the putative tetraalkyl Th(CH$_2$SiMe$_3$)$_4$(DME)$_x$. However, without convincing spectroscopic evidence, it is impossible to rule out a salt metathesis route wherein 2 equivalents of LiCH$_2$SiMe$_3$ deprotonate H$_2$[XA$_2$] and the resulting product react either with ThCl$_2$(CH$_2$SiMe$_3$)$_2$(DME)$_x$ to form [XA$_2$]Th(CH$_2$SiMe$_3$)$_2$ or ThCl$_4$(DME)$_2$ to give [XA$_2$]ThCl$_2$, which could then react with the remaining 2 equivalents of LiCH$_2$SiMe$_3$. If this chemistry indeed proceeds via the thermally unstable Th(CH$_2$SiMe$_3$)$_4$(DME)$_x$, this would represent one of the few examples of an organoactinide pincer complex being synthesized by alkane elimination, a method that is used extensively with rare earth and transition metals due to an abundance of accessible homoleptic metal alkyl starting materials. Notably, the relatively large Th$-$C$-$Si bond angles (126.8(3) and 127.6(3) degrees) in[XA$_2$]Th(CH$_2$SiMe$_3$)$_2$ are consistent with possible C$-$H$-$Th $\alpha$-agostic interactions. This proposal is corroborated by the low average coupling constant ($^1J_{C,H}$ = 102 Hz, toluene-$d_8$ at 50°C) for the methylene groups [56].

The related dibenzyl complex [XA$_2$]Th(CH$_2$Ph)$_2$, **23**, can also be generated in moderate yield (56%) by the straightforward reaction of [XA$_2$]ThCl$_2$(DME) with 2 equivalents of the benzyl Grignard PhCH$_2$MgCl; it was later revealed that the reason for the low yield is a competitive transmetallation reaction that affords [XA$_2$]Mg(DME) [57]. In an attempt to synthesize an organothorium cation, a single equivalent of B(C$_6$F$_5$)$_3$ was added to [XA$_2$]Th(CH$_2$Ph)$_2$; multinuclear NMR spectroscopy (e.g., $^{19}$F $\Delta\delta_{m,p}$ = 3.93, $^{11}$B $\delta$ = $-$11.6) established that the product [(XA$_2$)Th ($\eta^1$-CH$_2$Ph)][$\eta^6$-PhCH$_2$B(C$_6$F$_5$)$_3$], **24**, contains a stabilizing $\eta^6$-bound arene (Scheme 7.14) [58]. This product represents the first noncyclopentadienyl actinide alkyl cation.
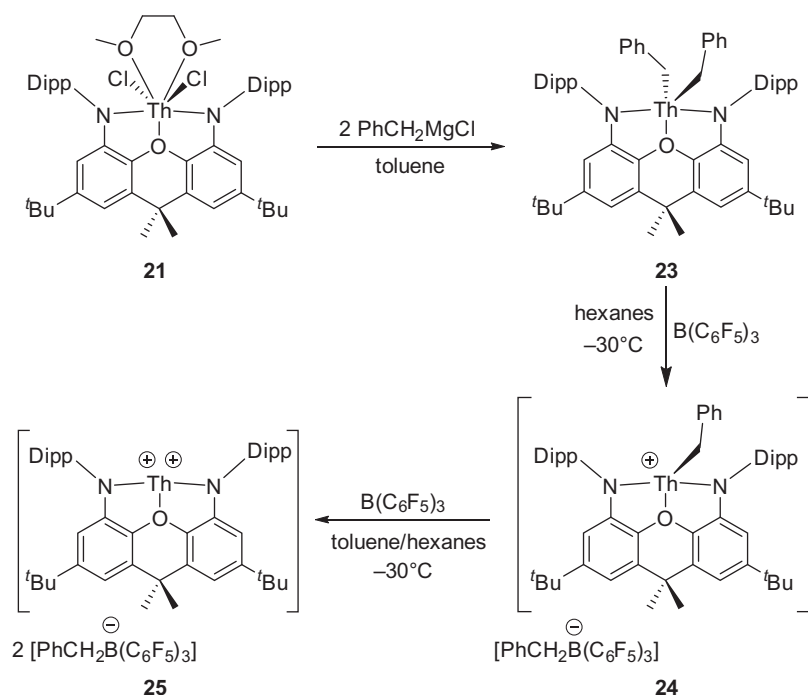


**SCHEME 7.14** Synthesis of mono- and dicationic thorium complexes **24** and **25**.

Remarkably, a second equivalent of B(C$_6$F$_5$)$_3$ can be added to [(XA$_2$)Th($\eta^1$-CH$_2$Ph)][$\eta^6$-PhCH$_2$B(C$_6$F$_5$)$_3$], to produce an exceedingly rare example of an actinide dication [(XA$_2$)Th][$\eta^6$-PhCH$_2$B(C$_6$F$_5$)$_3$]$_2$, **25** [58]. X-ray crystallography showed that both benzyl borate anions are coordinated to thorium via an $\eta^6$-interaction of the benzyl groups (Fig. 7.3). Unfortunately, it was not possible to study this unique complex by solution state spectroscopy, as it exhibits violent reactivity with conventional solvents. It is important to note that only a handful of dications have been produced via double ligand abstraction [59$-$61], and the resulting cations are often stabilized by an external Lewis base.
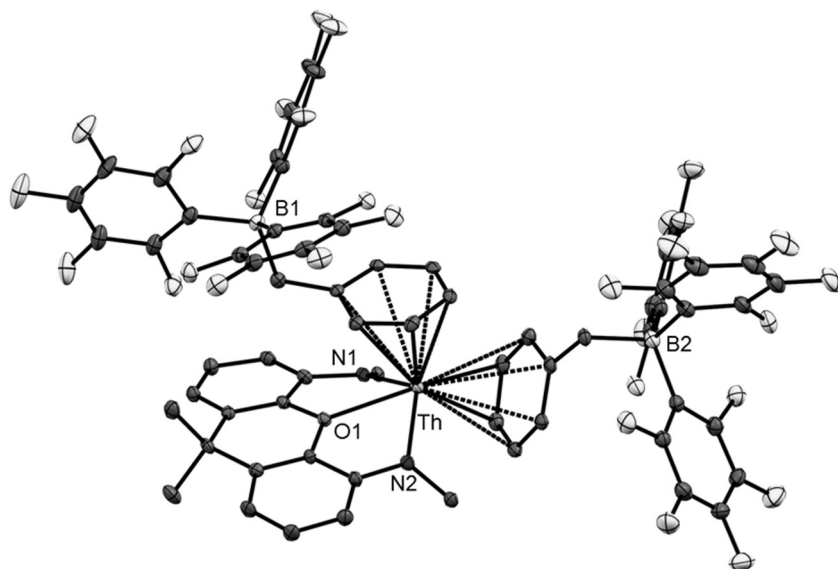
**FIGURE 7.3** X-ray crystal structure of ion pair **25**; thermal ellipsoids are drawn at 30% probability level, H-atoms omitted for clarity.

In an effort to circumvent the coordination of the benzyl borate anions, $[CPh_3][B(C_6F_5)_4]$ was used as an alkide abstraction reagent with both $[XA_2]Th(CH_2Ph)_2$ and $[XA_2]Th(CH_2SiMe_3)_2$ (Scheme 7.15) [62]. However, when the reaction was performed in benzene or toluene, the resulting products $[(XA_2)Th(CH_2SiMe_3)(\eta^6\text{-arene})][B(C_6F_5)_4]$ (arene = $C_6H_6$, toluene), **26**, and $[(XA_2)Th(\eta^2\text{-CH}_2Ph)(\eta^6\text{-C}_6H_5Me)][B(C_5F_6)_4]$, **27**, feature a solvent molecule coordinated in an $\eta^6$ fashion similar to that described earlier (Fig. 7.4).
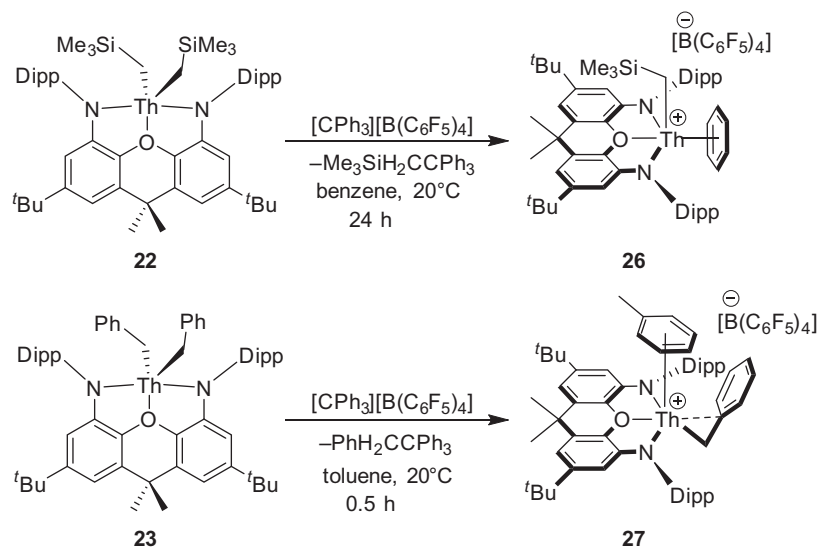


**SCHEME 7.15** Synthesis of organothorium cations **26** and **27** via reaction of complexes **22** and **23** with $[CPh_3][B(C_6F_5)_4]$.
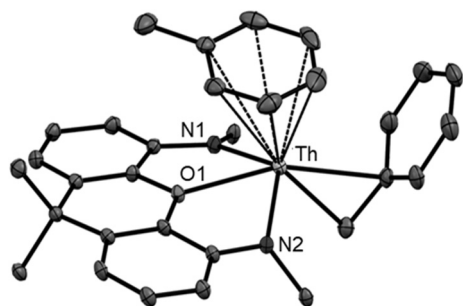


**FIGURE 7.4** X-ray crystal structure of complex **27**; thermal ellipsoids are drawn at 30% probability level, H-atoms are omitted for clarity.

Compounds **24**, **26**, and **27** were tested for ethylene polymerization, but no reactivity was observed, presumably because the strong π-arene coordination precludes alkene binding to the metal center [58]. This arene coordination motif has been shown to be preferred in less sterically encumbered cationic species, especially those with noncyclopentadienyl ligands. Thus, while particularly rigid pincer ligands are capable of supporting robust organoactinide complexes, cationic variants thereof appear prone to tight arene binding which can render them chemically inert [62].

Emslie and coworkers [63,64] have also explored the ability of their xanthene-based diamido pincer ligand to stabilize uranium species. Specifically, $[(XA_2)UCl_2(\mu\text{-}Cl)][K(DME)_3]$, **28**, an "ate" complex via reaction of $K_2(DME)_x[XA_2]$ and $UCl_4$, was prepared [64]. This complex was alkylated with 2 equivalents of (trimethylsilyl)methyl lithium and neopentyllithium to afford $[XA_2]U(CH_2SiMe_3)_2$, **29**, and $[XA_2]U(CH_2CMe_3)_2$, **30**, respectively (Scheme 7.16) [63]. Moreover, the reported compounds exhibit unusual transmetallation reactivity, with alkyl groups ($-CH_2SiMe_3$ and $-CH_2CMe_3$) exchanging at the metal center. This alkyl exchange activity, which eliminates an alkyl lithium instead of a lithium halide salt, parallels a salt metathesis reaction. Details on the proposed mechanism of exchange were presented, and while the putative mixed-trialkyl uranium complex was not detected, both $[Li(THF)_x]$ $[(XA_2)U(CH_2SiMe_3)_3]$ and $[Li(DME)_3][(XA_2)UMe_3]$ were identified as trialkyl lithium "ate" complexes, lending support to a stepwise transmetallation mechanism initiated by nucleophilic attack of LiR at the electropositive uranium center. This alkyl ligand exchange sequence was also observed in the analogous thorium complexes where evidence of the mixed-alkyl species $[XA_2]Th(CH_2SiMe_3)(CH_2Me_3)$ was provided by multinuclear NMR spectroscopy. Intriguingly, complete exchange from **22** to $[XA_2]Th(CH_2CMe_3)_2$ was obtained with an excess of $LiCH_2CMe_3$ (15 equivalents), but the addition of 2.2 equivalents of the same $LiCH_2CMe_3$ reagent gave a 1:1:3:1 mixture of $[XA_2]Th(CH_2CMe_3)_2$, $[XA_2]$ $Th(CH_2SiMe_3)(CH_2CMe_3)$, and the corresponding organolithium reagents ($LiCH_2SiMe_3$ and $LiCH_2CMe_3$) [63].
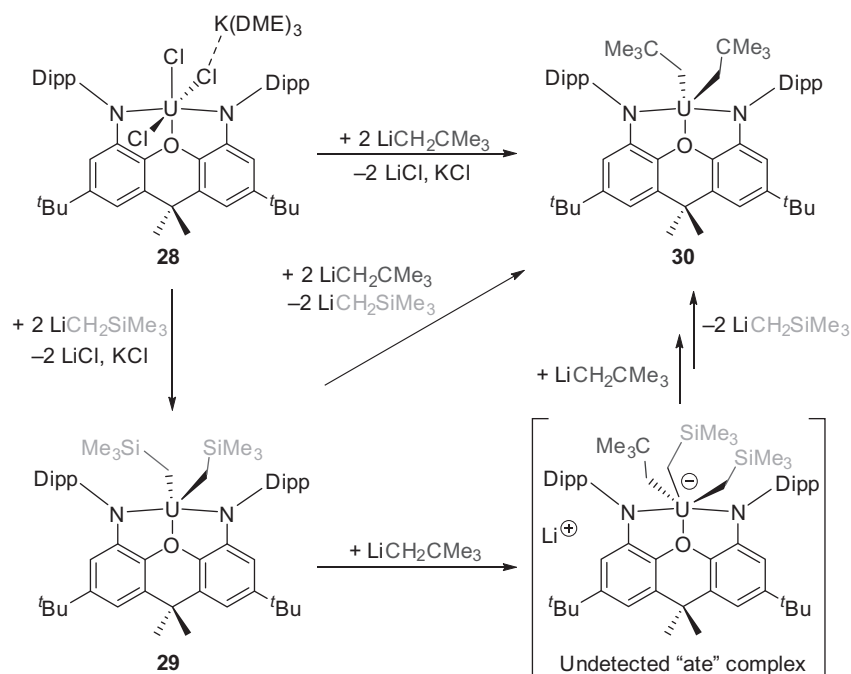


**SCHEME 7.16** Alkyl-exchange pathway in dialkyl uranium complexes **29** and **30**; light gray = $CH_2SiMe_3$, dark gray = $CH_2CMe_3$.

A sulfur analogue of the $XA_2$ scaffold, featuring a thioether linkage in the backbone was recently developed, creating a new *NSN* pincer $TXA_2$ ($TXA_2$ = 4,5-bis(2,6-diisopropylanilino)-2,7-di-tert-butyl-9,9-dimethylthioxanthene) [64]. The mixed hard−soft donor properties of the $TXA_2$ ligand were examined in comparison to the *NON* framework of $XA_2$ by preparing several U(III) and U(IV) complexes of each. Addition of a DME solution of $Li_2(DME)_2[TXA_2]$ to $UCl_4$ produced the dark red "ate" complex $[Li(DME)_3][(TXA_2)UCl_3]$, **31**, in 42% yield (Scheme 7.17). A solid-state comparison of **31** and **28** identified several interesting features. For example, the U−S distances of 2.763(2) Å and 2.779(2) Å (two independent molecules exist in the unit cell) in $[Li(DME)_3][(TXA_2)UCl_3]$ are substantially shorter than other previously reported neutral U−S contacts [44,45]. Interestingly, the backbone of the $TXA_2$ ligand is bent into a "butterfly conformation" (C−S−C and C−S−U angles of 97−98 degrees), a sharp contrast to the planar core of the more rigid $XA_2$ ligands (C−O−C and C−O−U angles of 118−120 degrees). The bending of the $TXA_2$ ligand appears to persist in the solution state, as NMR spectroscopic data indicates a $C_s$ symmetric structure, whereas the planar $XA_2$ complex exhibits $C_{2v}$ symmetry in solution.
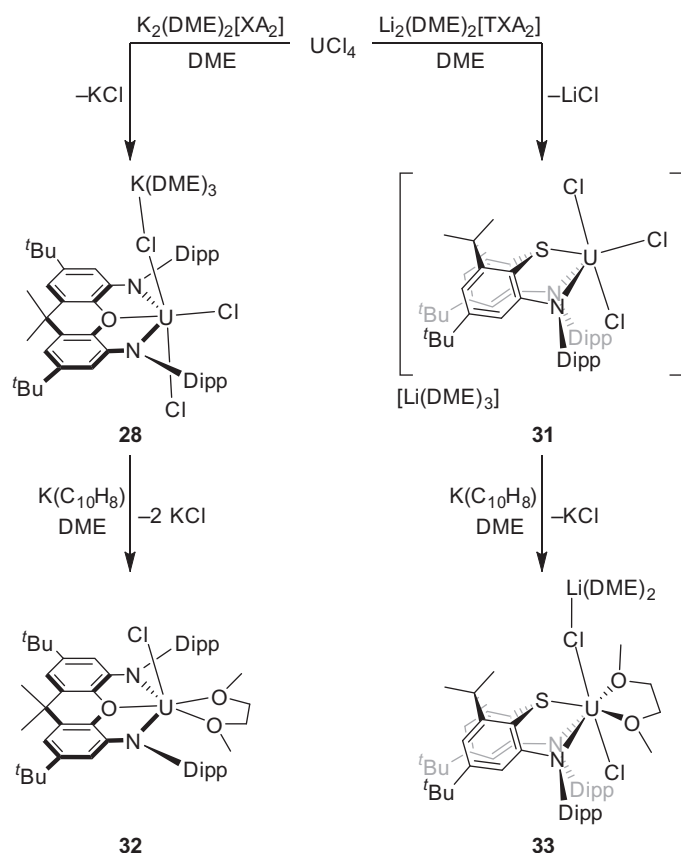
The cyclic voltammograms of both **28** and **31** showed irreversible reductions. Chemical reduction with 1 equivalent of K(naphthalenide) in DME afforded the U(III) products [XA$_2$]UCl(DME), **32**, and [(TXA$_2$)UCl(DME)($\mu$-Cl)][Li(DME)$_2$], **33**, (the latter decomposes in solution at temperatures above $-30°$C), which were crystallographically characterized (Scheme 7.17). Similar to the tetravalent complexes, the trivalent species **33** contained a bent *NSN* ligand backbone compared to the planar *NON* ligand in **32**. DFT calculations suggest a greater degree of covalency is present in the U$-$SAr$_2$ bond than that of than the U$-$OAr$_2$. This finding is supported experimentally by solid-state data which indicates an uncharacteristically short U$-$S distance [2.825(1) Å] [64].

Emslie and coworkers have clearly established the ability of the XA$_2$ and TXA$_2$ pincer ligands to serve as suitable platforms for actinide metals, with demonstrated thermal stability of the resultant organometallic complexes rivaling that observed for Cp.

A similar series of dianionic *NON* pincer complexes, some of which have been exploited as catalysts in several common chemical transformations, have been reported by the Leznoff group. A diamidosilyl ether ligand [$^{tBu}$NON] ([$^{tBu}$NON] = {Me$_3$CN(SiMe$_3$)$_2$)$_2$O) was used in the synthesis of the dimeric halide complexes [($^{tBu}$NON)AnCl$_2$]$_2$ (An = U, **34-U**; Th, **34-Th**) via a salt metathesis reaction of Li$_2$[$^{tBu}$NON] and AnCl$_4$ [65]. Treatment of [($^{tBu}$NON]AnCl$_2$]$_2$ with 2 equivalents of C$_3$H$_5$MgCl and LiCH$_2$SiMe$_3$ afforded [$^{tBu}$NON]An(CH$_2$SiMe$_3$)$_2$ (An = U, **35-U**; Th, **35-Th**) and [$^{tBu}$NON]An(C$_3$H$_5$)$_2$ (An = U, **36-U**; Th, **36-Th**), respectively. Additionally, in [$^{tBu}$NON]AnCp*Cl (An = U, **37-U**; Th, **37-Th**) one chloride group was replaced with a Cp* ligand (Cp* = C$_5$Me$_5^-$) by reaction of **34** with NaCp*. Although complexes **37** proved too bulky to accommodate another Cp*, addition of MeMgBr afforded the mixed Cp*/Me complexes [$^{tBu}$NON]AnCp*Me (An = U, **38-U**; Th, **38-Th**) (Scheme 7.18) [65].

**SCHEME 7.18** Synthesis of organometallic complexes of an *NON* pincer ligand.

Following the success of their [$^{tBu}$NON] ligand, An(IV) complexes of diamidosilyl ether ligands featuring mesityl [$^{Mes}$NON] and Dipp [$^{Dipp}$NON] ([$^{Mes}$NON] = (2,4,6-Me$_3$C$_6$H$_2$N(SiMe$_2$))$_2$O, [$^{Dipp}$NON] = (2,6-$^i$Pr$_2$C$_6$H$_3$N(SiMe$_2$))$_2$O) groups on the amido nitrogen atoms were prepared [66]. Similarly, a diamido ether ligand with ethylene backbone linkages [$^{Dipp}$NCOCN] was also studied ([$^{Dipp}$NCOCN] = (2,6-$^i$PrPhN(CH$_2$CH$_2$))$_2$O). All of these ligands support actinide halide "ate" complexes (**39−41**) formed from dilithiated ligand in THF (Chart 7.3), and **39** and **41** can be used as viable precursors to monomeric, salt-free organometallic complexes [66].



**CHART 7.3** Uranium and thorium "ate" complexes of *NON* pincer ligands.

For further details on the catalytic reactivity of these compounds and their derivatives, refer to Section 7.4.

### 7.3.3.2 SCS/NCN *Ligands*

In closely related work by Ephritikhine [36,67−70], Cavell [71], and Liddle [47,48,72−83], dianionic pincer carbene ligands [(Ph$_2$P = S)$_2$C]$^{2−}$ (SCS) and [(Ph$_2$P = NR)$_2$C]$^{2−}$ ($^R$BIPM; R = Mes, Dipp, SiMe$_3$) were utilized with the intention of studying actinide−carbon multiple bonding. The first contributions from Ephritikhine focus on *SCS* ligand constructs, though the field is now dominated by Liddle's work with derivatives of BIPM, a dianionic *NCN* ligand with flanking phosphinimine donors first introduced by Cavell [84] and Stephan [85]. Actinide carbene chemistry experienced a renaissance within the *SCS/NCN* pincer context after a period of dormancy following the first uranium carbene ($\eta^5$-C$_5$H$_5$)$_3$U = CHP(CH$_3$)$_2$(C$_6$H$_5$) reported by Gilje in 1981 [86]. This section focuses on the synthesis and reactivity of actinide pincer carbene complexes; for a theoretical discussion, the interested reader is directed to the source material. Select references that are particularly noteworthy and rich in theoretical detail include: (1) inverse-*trans*-influence operative in mid-valent (4 + ) cerium, thorium, and uranium bis(carbene) complexes [75], (2) computational assessment of covalency in isostructural cerium(IV) and uranium(IV) carbene complexes [76], and (3) comparative DFT study of M = C double bonds in uranium carbene complexes with lanthanide, thorium, and transition metal congeners [47]. Taken together, these theoretical contributions complement the experimental results provided in the following discussion.

In pincer carbene complexes bearing ligands with phosphorano donors, the uranium center plays host to a variety of coordination environments. This allows for careful study of the organometallic U−C bond distances by X-ray crystallography, which range from 2.327(3) Å in U(SCS)(BH$_4$)$_2$(THF)$_2$, **42**, to 2.48(1) Å in [Li(OEt$_2$)]$_2$[SCS]$_3$U, **43** [68]. The

double bond character of these carbene complexes is evident given meaningful comparisons within a mixed-ligand system [SCS]U(HSCS)(NEt$_2$), **44**, where one of the central carbon atoms is protonated, and serves as a monoanionic methanide donor. Bond distances vary markedly in this case: U−C = 2.395(5) Å and 2.819(5) Å were observed for the double and single bonds, respectively [36]. The electronic structures of uranium carbenes were also considered. In a comparative DFT study [36], the lower-energy 5$f$ atomic orbitals of tetravalent uranium engage the nucleophilic lone pair on carbon more effectively than higher energy 6$d$ orbitals of the analogous transition metal (Zr) complex.

The *SCS* ligand set presents a dianionic central methandiide donor, which under the appropriate conditions cooperates with established salt metathesis strategies. For the uranium complex [SCS]UCl(THF)(μ-Cl)$_2$Li(THF)$_2$, **45** [36], salt metathesis from UCl$_4$ worked well. Notably, amine elimination from the combination of H$_2$C(Ph$_2$PS)$_2$ and U(NEt)$_4$ in THF afforded a mixture of the pincer diamide complex [SCS]U(NEt$_2$)$_2$, **46**, and the diligand species [SCS]$_2$U(THF)$_2$, **47-U** (Scheme 7.19) [36]. The tetravalent mono-, bis-, and triligand "ate" complexes were generated through salt metathesis reactions of uranium and thorium halides. Altogether, the structural variety of these compounds is far reaching [36,72,74].



SCHEME 7.19 Synthesis of *SCS*-based carbene actinide pincer complexes.
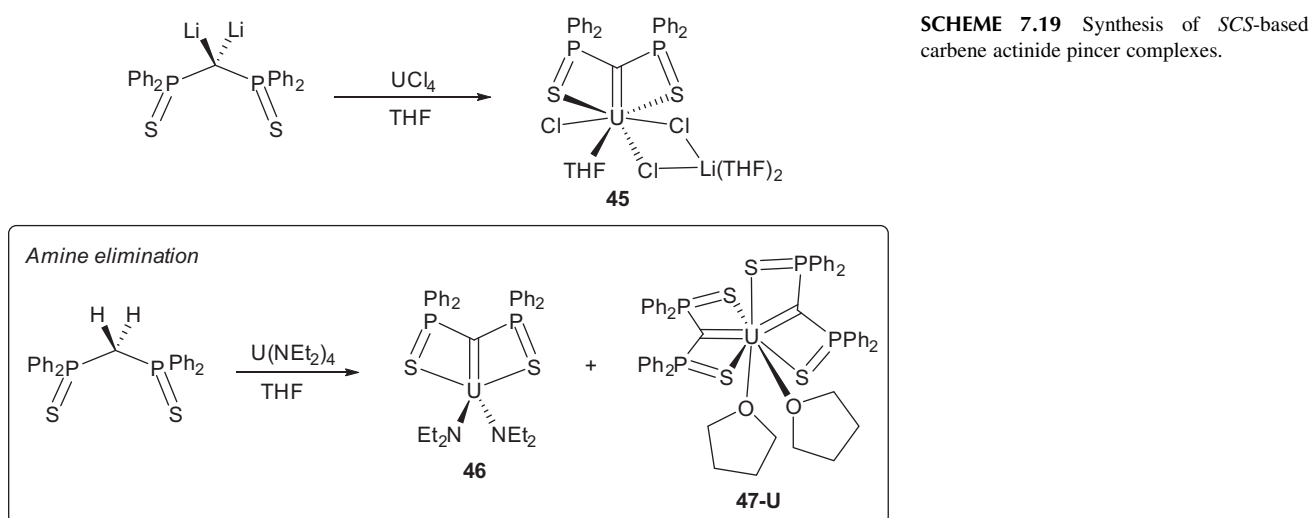
In a review by Edelmann [3], the $f$-orbital manifold is described as "buffering" the reactivity of these reactive carbene lone pairs. Intriguingly, thermolysis of **47-U** in pyridine, as reported by the Ephritikhine, resulted in the formation of [SCS]U(CS(Ph$_2$PS)$_2$)(py), **48**, by formal addition of one S atom across the U = C double bond (Scheme 7.20) [36]. Alternatively, when **47-U** was reacted with UCl$_4$, 2 equivalents of [SCS]UCl$_2$(THF)$_2$, **49**, a LiCl-free analogue of "ate" complex **45**, was produced [36]. Notably, the carbene functionality in [SCS]$_2$Th(DME), **47-Th**, makes for a capable nucleophile, as demonstrated in the C−C coupling reaction with benzophenone (Ph$_2$CO) (Scheme 7.21) [87]. Ultimately, seminal work by Ephritikhine and coworkers has helped to reinvigorate the study of actinide carbene complexes.



SCHEME 7.20     Addition of an S atom across U = C.

**47-Th**
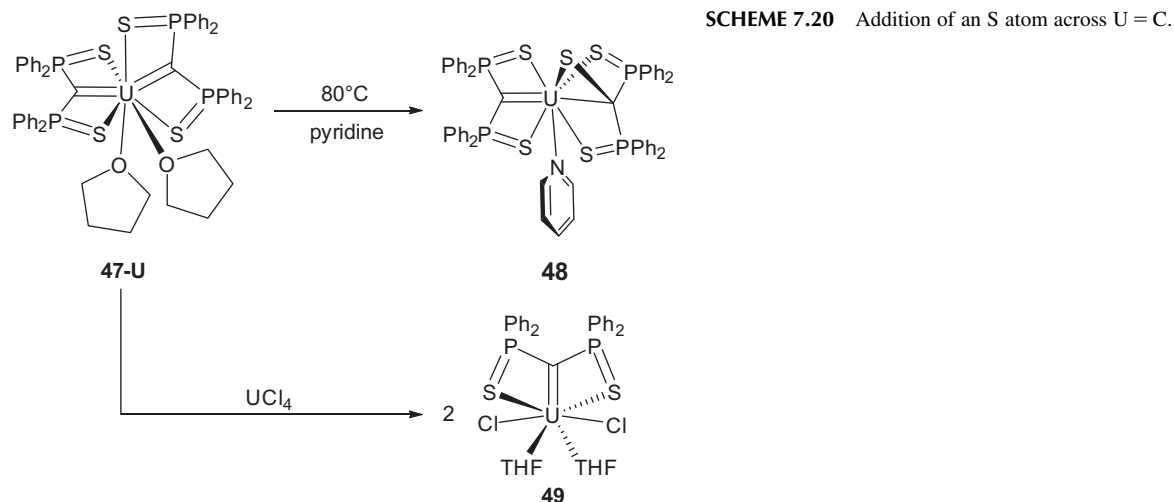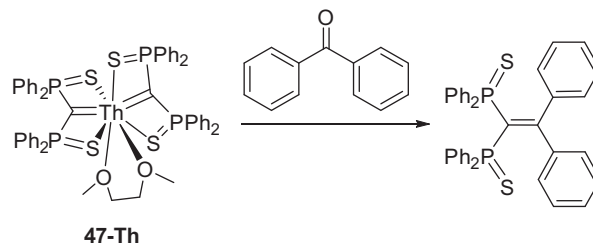
**SCHEME 7.21** C−C coupling of an *SCS* pincer ligand and benzophenone.

Following the pioneering work of Ephritikhine and Cavell, Liddle produced an impressive body of work dealing with carbon−actinide multiple bonding by developing actinide pincer carbene complexes where the ligands bear a dianionic methandiide group: $[C(PPh_2NR)_2]^{2-}$ (R = 2,6-$^i$Pr$_2$C$_6$H$_3$, $^{Dipp}$BIPM, 2,4,6-Me$_3$C$_6$H$_2$, $^{Mes}$BIPM, and SiMe$_3$, $^{TMS}$BIPM) [72−83]. The variant bearing SiMe$_3$-appended phosphinimine donors ($^{TMS}$BIPM) has received the most attention. Structural modification to the BIPM ligand was carried out as a method of controlling the reactivity of the actinide carbene linkage. The methylene bridge of the generic proteo H$_2$C[(Ph$_2$P = NR)$_2$] ligand was amenable to metathesis reactions following double deprotonation with alkali metal reagents. For example, Li$_2$[$^{Mes}$BIPM] was combined with UCl$_4$(THF)$_3$ to afford [$^{Mes}$BIPM]UCl$_2$(THF)$_2$, **50** (56% yield), a species which was prone to ligand scrambling and other decomposition pathways [47]. Opting for the bulkier $^{Dipp}$BIPM ligand congener, UCl$_4$(THF)$_3$ was combined with Li$_2$[$^{Dipp}$BIPM](tmeda) (tmeda = *N*,*N*,*N*′,*N*′-tetramethylethylenediamine) to afford the "ate" complex [$^{Dipp}$BIPM]U (μ-Cl)$_4$Li$_2$(OEt$_2$)(tmeda), **51**, in 45% yield [47]. Heating complex **51** offered an alternate pathway for forming uranium carbene dichloride complexes, specifically [$^{Dipp}$BIPM]UCl$_2$(THF)$_2$, **52**. The increased steric bulk of complex **52** proved to stabilize the carbene more effectively than the $^{Mes}$BIPM variant, which allowed reactivity studies to be undertaken.

A further testament to the increased stability of the $^{Dipp}$BIPM ligand was showcased by chemical oxidation. A rare example (*vide infra*) of a pentavalent uranium complex [$^{Dipp}$BIPM]UCl$_2$(μ-Cl)$_2$Li(THF)$_2$, **53**, was generated through addition of 0.5 equivalent of molecular iodine (I$_2$) to **51**. Remarkably, oxidation of **51** with LiO$^t$Bu and I$_2$ resulted in a U(VI) complex that features four σ-bonds. Liddle and coworkers have emphasized the role of multiply bonded ligands in stabilizing high-valent actinide complexes, still, the hexavalent species [κ$^2$-*C*,*N*-$^{Dipp}$BIPM]U(O$^t$Bu)$_3$I, **54**, contains only a single carbene donor, with the remaining ligands σ-bound. The stability of complex **54** was reinforced by the lack of reactivity with aldehydes. This family of compounds provided an opportunity to draw meaningful comparisons between the reactivity of U(IV) and U(VI) carbenes, as [$^{Dipp}$BIPM]UCl$_2$(THF)$_2$, **52**, reacted readily with benzaldehyde to afford the substituted alkene (Scheme 7.22) [47].

In a similar way, the generation of [$^{TMS}$BIPM]AnCl(μ-Cl)$_2$Li(THF)$_2$, An = U, **55**; [74] Th, **56** [71], was achieved by combining UCl$_4$(THF)$_3$ or ThCl$_4$(DME)$_2$ with the dilithiated ligand salt Li$_2$[(Ph$_2$P = NR)$_2$C]. Complexes **55** and **56** serve as an entry point to organometallic complexes through the addition of 2 equivalents of LiCH$_2$SiMe$_3$, affording [$^{TMS}$BIPM]An(CH$_2$SiMe$_3$)$_2$, An = U, **57-U**; [80] Th, **57-Th** [75] (Scheme 7.23). Complex **57-U** was susceptible to protonolysis, reacting with trityl amine (Ph$_3$CNH$_2$) and bipy (bipy = 2,2′-bipyridine) to provide facile access to the terminal uranium *cis*-imido complex [$^{TMS}$BIPM]U(NCPh$_3$)(bipy), **58** [80]. Notably, the geometry of the imido ligand was altered via addition of 2 equivalents of DMAP (DMAP = 4-dimethylaminopyridine), which promoted *cis* to *trans* isomerization relative to the carbene functionality, ultimately giving [$^{TMS}$BIPM]U(NCPh$_3$)(DMAP)$_2$, **59** [80]. This work by Liddle, together with the recent study on the inverse-*trans*-influence (ITI) in the actinide bis(carbenes) [$^{TMS}$BIPM]$_2$An, An = U, **60-U**; Th, **60-Th** [75], has provided greatly enhanced understanding of the interactions between actinides and multiply-bonded ligands.

The "metallo-Wittig" reaction was applied in C−C bond-forming transformations with **55**, as well as the higher-valent uranium oxo species [$^{TMS}$BIPM]UCl$_2$(O), **61** [83], providing an expanded substrate scope that includes substituted aldehydes (RCHO, R = phenyl, 9-anthracene) (Schemes 7.23 and 7.24) [47,73,83]. Notably, reaction of complex **55** with the bulky ketone Ph$^t$BuCO showed limited efficacy in C−C coupling, but did produce the dimeric complex [($^{TMS}$BIPM)UCl(μ-Cl)(OCPh$^t$Bu)]$_2$, **62** (Scheme 7.23) [73]. These preliminary examples demonstrate promise for a variety of "C for O" metathesis reactions, along with small molecule activation across reactive U = C bonds.

Liddle et al. [74] recently reported the synthesis of an unusual, solvent-free, pentavalent uranium pincer complex. While the first uranium carbene complexes were defined by short organometallic bonds between carbon and tetravalent uranium, prior to 2011 uranium(V) carbenes were notably absent from the literature. One electron oxidation of the U (IV) complex [$^{TMS}$BIPM]UCl(μ-Cl)$_2$Li(THF)$_2$, **55**, with 0.5 equivalent of I$_2$, gave [$^{TMS}$BIPM]UCl$_2$I, **63**, in 45% yield (Scheme 7.25). Direct structural comparisons between the tetra- and pentavalent uranium carbene complexes were
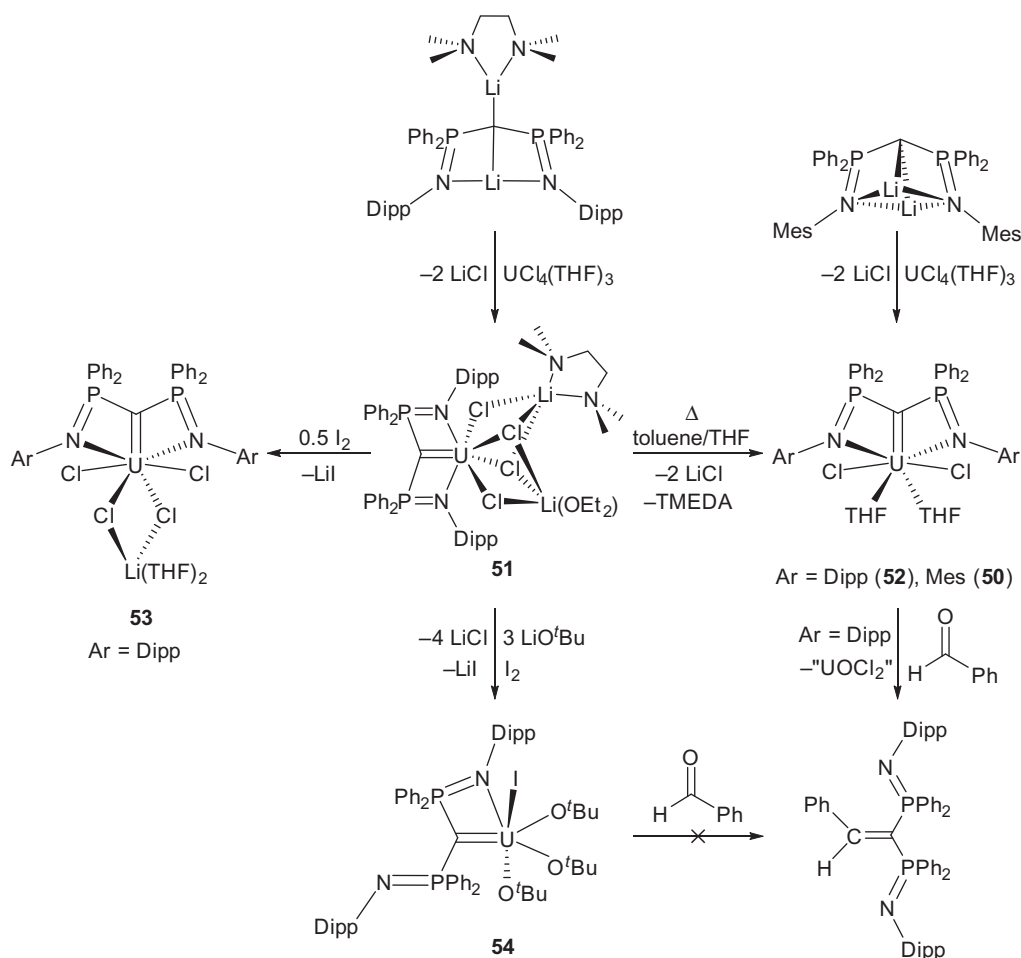
**SCHEME 7.22**    Synthesis and reaction chemistry of *NCN*-supported uranium carbene complexes.

made possible, for the first time, by X-ray crystallography. Notably, oxidation of the uranium center resulted in contraction of the U = C bond from 2.310(4) Å in **55** to 2.27(1) Å in **63** [74]. More recently, Liddle and colleagues have pushed the limits of actinide element multiple bonding [47], introducing a single uranium complex which exhibits multiple-bonding interactions to three different elements (C, N, and O) [79]. The pincer carbene ligand ($^{TMS}$BIPM) accounts for the covalent organometallic double bond, while terminal oxo and imido groups complete the coordination sphere. From [$^{TMS}$BIPM]UCl($\mu$-Cl)$_2$Li(THF)$_2$, **55**, the carbene dialkyl [$^{TMS}$BIPM]U(CH$_2$Ph)$_2$, **64**, was generated by straightforward addition of benzyl potassium (KBn). Notably, this dibenzyl carbene species was the first disclosed for uranium, which, given the number of uranium carbene derivatives in the literature, represents an important step forward. Protonolysis of the carbene dialkyl using a bulky aromatic amine (MesNH$_2$, Mes = 2,4,6-Me$_3$C$_6$H$_2$) generated [($^{TMS}$BIPM)U(NMes)]$_2$, **65**, a bridging imido complex, in 92% yield.

Two-electron oxidation of complex **65** with tetramethylpiperidine-*N*-oxide (TEMPO) cleanly oxidized the tetravalent uranium center [U(IV)→U(VI)], affording the mixed carbene-oxo-imido complexes [($^{TMS}$BIPM)U(NMes)(O)]$_2$, **66**, and [$^{TMS}$BIPM]U(NMes)(O)(DMAP)$_2$, **67** (Scheme 7.25) [79]. Earlier reports have described the reactivity of uranium carbon double bonds in C—C coupling reactions giving substituted alkenes and uranyl complexes (*vide supra*). Here, the metathesis occurred exclusively at the imido site (N for O, as opposed to C for O metathesis), generating the uranyl carbene complex [$^{TMS}$BIPM]U(O)$_2$(DMAP)$_2$, **68**, and asymmetric carbodiimide ($^t$BuN = C = NMes) as the sole organic product (Scheme 7.25) [79].

The selective insertion chemistry outlined earlier has also been observed with thorium. As a showcase of selectivity, Liddle identified the ketimide ligand in [$^{TMS}$BIPM]Th(N(SiMe$_3$)$_2$)(N = CPh$_2$), **69**, as the locus of reactivity with unsaturated substrates [81]. The precursor dichloride complex [$^{TMS}$BIPM]ThCl$_2$, **70**, which was generated in situ by reaction between ThCl$_4$(DME)$_2$ and Li$_2$[$^{TMS}$BIPM], was immediately treated with KN(SiMe$_3$)$_2$ to afford [($^{TMS}$BIPM)Th((N(SiMe$_3$)$_2$)($\mu$-Cl)]$_2$, **71**, in 85% isolated yield (Scheme 7.26). Near-quantitative generation of the titular complex **69** was

**SCHEME 7.23** Synthesis and reaction chemistry of actinide "ate" complexes **55** and **56**.



**SCHEME 7.24** "C for O" metathesis.
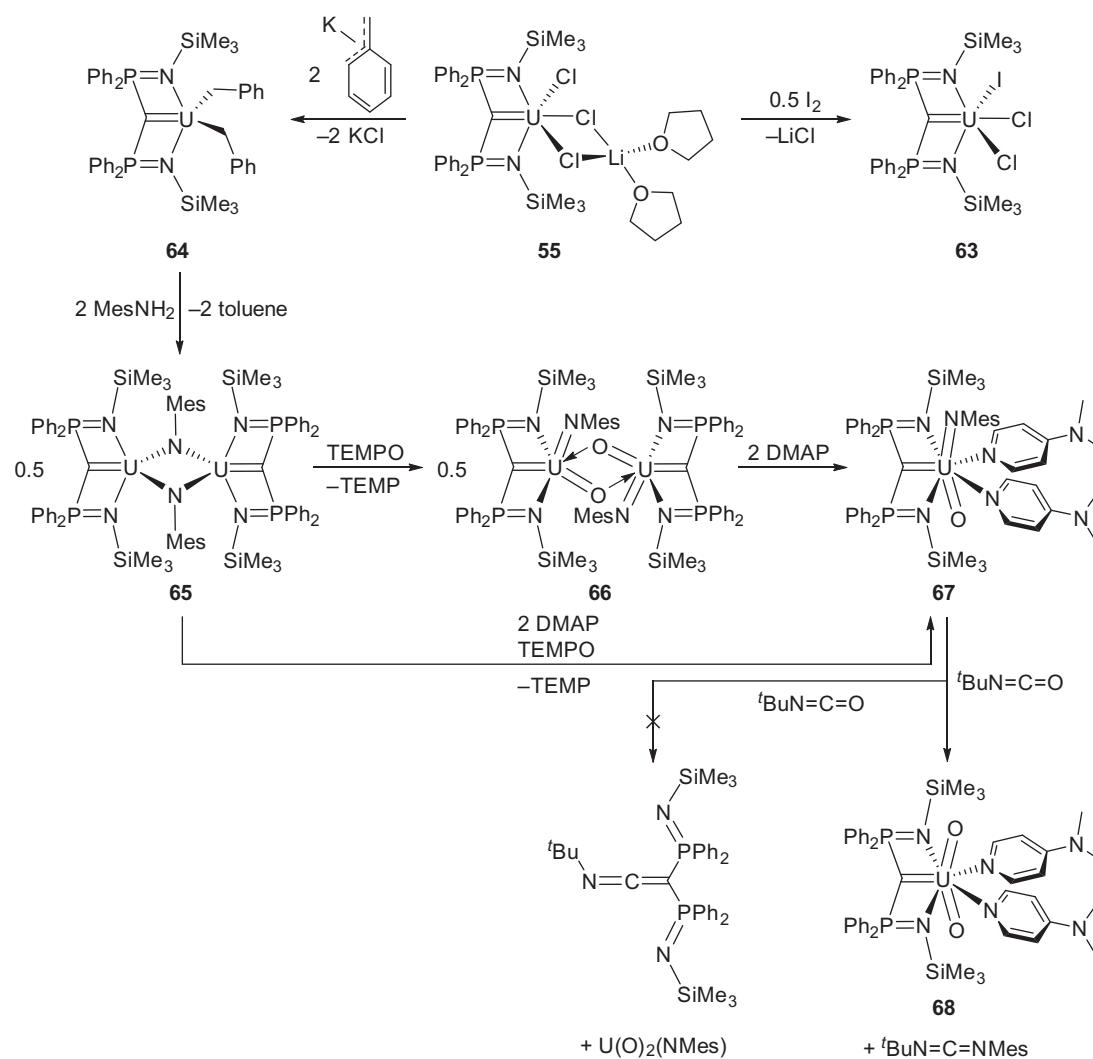
**SCHEME 7.25** Synthesis of *NCN* imido and oxo uranium complexes.
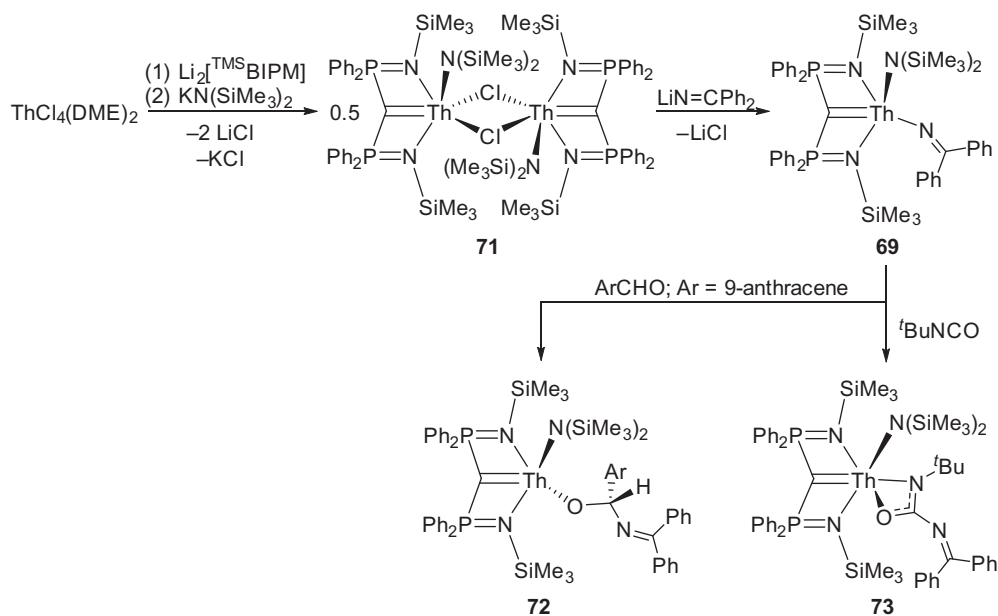


**SCHEME 7.26** Reaction of thorium ketimide **69** with isocyanates.

achieved by treatment of **71** with 2 equivalents of Li(N = CPh$_2$), resulting in intense coloration of the benzene solution. Given the $6d^05f^0$ electronic configuration of the tetravalent thorium complex **69**, such bright color must originate from the spin-allowed but orbital-forbidden p ⊥ (N) → π* (N = C) transition, and ligand-to-metal charge transfer, consistent with a previous report from Kiplinger detailing the molecular spectroscopy of uranium(IV) bis(ketimide) complexes [88].

As was the case in complex **67** (*vide supra*) [79], the presence of thorium carbene, amide, and ketimide ligands provided an opportunity to assess selective insertion chemistry. Specifically, complex **69** was treated with both 9-anthracene carboxaldehyde and *tert*-butylisocyanate (RN = C = O). In both cases the substrate reacted preferentially with the ketimide ligand over thorium carbene and amide functionalities, a surprising turn given that ketimide ligands are established inert spectators. Formation of the alkoxy complex [$^{TMS}$BIPM]Th(N(SiMe$_3$)$_2$)(OC(H)(NCPh$_2$)(C$_{14}$H$_9$)), **72**, was accompanied by the complete disappearance of absorptions in the UV/Vis spectrum, consistent with selective insertion of the C = O bond of 9-anthacene carboxaldehyde into the Th−N$_{ketimide}$ linkage. Similarly, the Th−N$_{ketimide}$ bond reacted with *tert*-butylisocyanate to form the thorium carbene amide ureate [$^{TMS}$BIPM]Th((N(SiMe$_3$)$_2$)(OC(N$^t$Bu) (NCPh$_2$)), **73** (Scheme 7.26) [81].

### 7.3.3.3  NNN *Ligands*

Similar to their chemistry with *NON* pincer complexes (Section 7.3.3.1), the Emslie group has also explored thorium chemistry with the previously reported BDPP ligand (BDPP = 2,6-bis(2,6-diisopropylanilidomethyl)pyridine), developed by McConville and coworkers [89−91] and originally used to support titanium, zirconium, and tantalum complexes. In order to pursue salt metathesis strategies, the lithiated ligand Li$_2$[BDPP] was synthesized by reaction of H$_2$[BDPP] with 2 equivalents of an alkyl lithium reagent (LiCH$_2$SiMe$_3$ or $^n$BuLi) [56]. The dichloride etherate complex [BDPP]ThCl$_2$(DME), **74**, can be synthesized in 51% yield by addition of Li$_2$[BDPP] to ThCl$_4$(DME)$_2$. Conversely, **74** can also be prepared by stirring ThCl$_4$(DME)$_2$ and 2 equivalents of LiCH$_2$SiMe$_3$ at −78°C for an hour, followed by dropwise addition of H$_2$[BDPP]. Alkylation of **74** using 2 additional equivalents of LiCH$_2$SiMe$_3$ resulted in the thermally robust (stable at 90°C in toluene solution for multiple days) organoactinide complex [BDPP]Th(CH$_2$SiMe$_3$)$_2$, **75** (Scheme 7.27) [56].
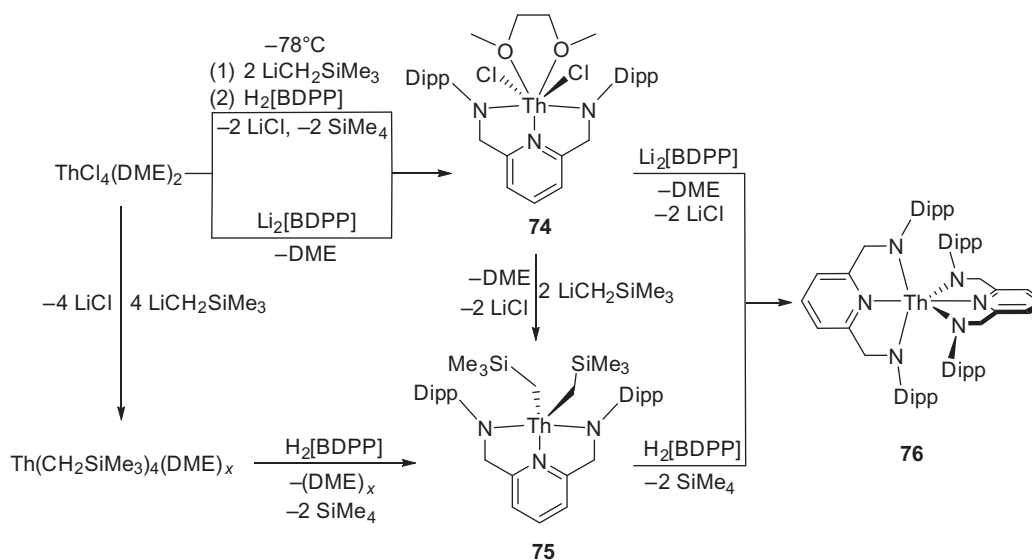


**SCHEME 7.27**    Synthesis of thorium complexes of an NNN pincer ligand.

Intriguingly, when 1 equivalent of Li$_2$[BDPP] was added to [BDPP]ThCl$_2$(DME), the diligand complex Th[BDPP]$_2$, **76**, was isolated. This reactivity contrasts that observed with the analogous XA$_2$ complex (XA$_2$ = 4,5-bis(2,6-diisopropylanilido)-2,7-di-*tert*-butyl-9,9-dimethylxanthene) which does not appear capable of accommodating a second pincer ligand [56].

In continuing the investigation of organothorium complexes, the Emslie group prepared the corresponding methyl and *n*-butyl complexes of BDPP, [Li(DME)][(BDPP)ThMe$_3$], **77**, and [BDPP]Th$^n$Bu$_2$, **78** (Scheme 7.28). Intriguingly, complex **78** was found to be exceedingly robust, while **77** readily cyclometalated at ambient temperature in solution giving [Li(DME)][(BDPP*)ThMe$_2$] (BDPP* = 2,6-NC$_5$H$_3$(CH$_2$NDipp)(CH$_2$N{C$_6$H$_3$$^i$Pr(CMe$_2$)-2,6}), **79**). Notably, the site of cyclometalation was the methine carbon of the Dipp isopropyl, as opposed to the more common methyl group [92].
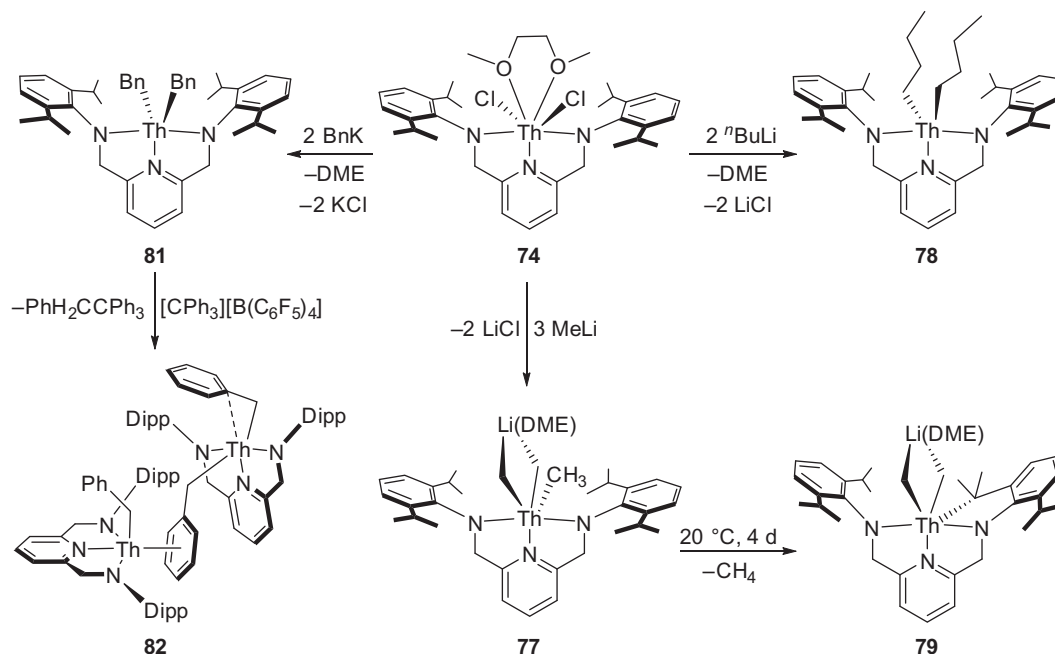


**SCHEME 7.28**   Preparation of a thermally robust dibutyl thorium complex and an unstable dimethyl analogue.

In an effort to install methyl groups without retaining lithium salts within the coordination sphere of the metal 2 equivalents of MeMgBr were reacted with [BDPP]ThCl$_2$(DME) in diethylether. Interestingly, the result of this reaction was revealed to be the product of a partial halide exchange reaction with MeMgBr, which exclusively afforded [(BDPP)ThX($\mu$-X)$_2$Mg(OEt$_2$)($\mu$-Me)]$_2$ (X = Br$_{0.73-0.87}$/Cl$_{0.13-0.27}$, **80**, as determined by X-ray crystallography (Fig. 7.5)), with no evidence of the desired product [BDPP]ThMe$_2$ [57]. Although halide exchange with Grignard reagents is not uncommon with actinide complexes [93], such incomplete alkylation is generally viewed as problematic. This unusual complex is thus important as it sheds light upon the mechanism of halide exchange [57].
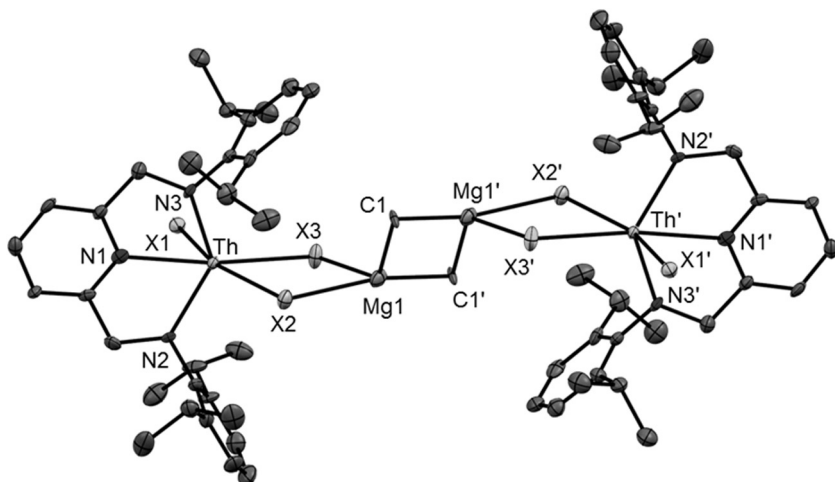


**FIGURE 7.5**   X-ray crystal structure of [(BDPP) ThX($\mu$-X)$_2$Mg(OEt$_2$)($\mu$-Me)]$_2$, **80**; thermal ellipsoids are drawn at 30% probability level, H-atoms are omitted for clarity, X = Br or Cl,$'$ = −x, − y, − z.

Finally, these organothorium complexes were investigated with respect to their propensity to form thorium cations [62]. In contrast to the chemistry observed with the $XA_2$ scaffold, which forms mononuclear cationic complexes (Section 7.3.3.1), the resulting cation bearing the BDPP ligand was dinuclear. Reaction of dibenzyl [BDPP]Th($\eta^2$-$CH_2Ph$)($\eta^3$-$CH_2Ph$), **81** with between 0.5 and 1.0 equivalent of $[CPh_3][B(C_6F_5)_4]$ resulted in dinuclear species [(BDPP)Th($\eta^2$-$CH_2Ph$)($\mu$-$\eta^1$:$\eta^6$-$CH_2Ph$)Th($\eta^1$-$CH_2Ph$)(BDPP)][$B(C_6F_5)_4$], **82**, which possesses a benzyl group that bridges between cationic and neutral thorium centers. Reminiscent of the arene coordination seen with the $XA_2$ system, in which a solvent molecule of benzene was $\eta^6$-coordinated to thorium, the cationic metal center in **82** is bound to the benzyl ligand in an $\eta^6$-fashion. Furthermore, reaction of [BDPP]Th($\eta^2$-$CH_2Ph$)($\eta^3$-$CH_2Ph$) with 2 equivalents of $[CPh_3][B(C_6F_5)_4]$ extruded two molecules of $PhH_2CCPh_3$. Although this organic by-product implies formation of a dication similar to **25**, produced from the reaction of $[XA_2]Th(CH_2Ph)_2$ and 2 equivalents of $B(C_6F_5)_3$ (Section 7.3.3.1), the authors were unable to isolate it [62].

Diaconescu and colleagues [94] employed the BDPP ligand with uranium, during which they prepared a family of U (IV) complexes starting from $UI_3(THF)_4$. Although this ill-defined process did not render it possible to identify all of the metal-containing products, it was reasonably postulated that a disproportionation reaction was operative, and hence responsible, for generating the well-behaved tetravalent products. When $[Li(OEt_2)]_2[BDPP]$ was added to $UI_3(THF)_4$ only the U(IV) diligand complex $U[BDPP]_2$, with no sign of $[BDPP]UI_2$ (which could presumably be generated upon reaction with $UI_4(solvent)_x$), was observed. Attempts to synthesize organouranium species via in situ generation of the uranium trialkyl at low temperature, followed by addition of $H_2[BDPP]$ in an alkane elimination reaction, provided access to $[BDPP]U(CH_2Ph)_2$, **83** and $[BDPP]UI(CH_2Ph)$, **84** (Scheme 7.29).
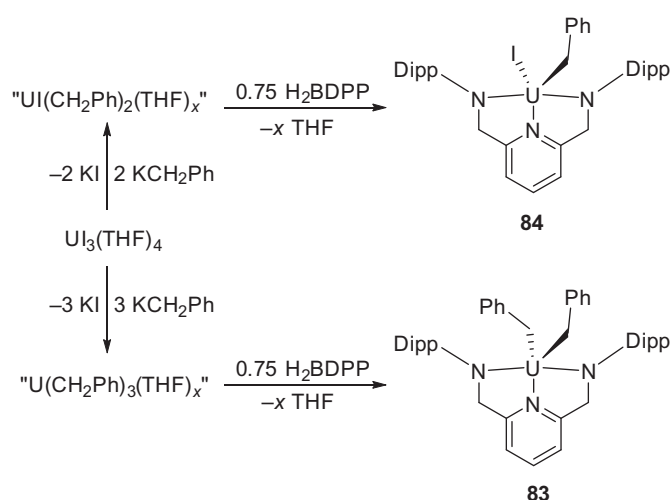


**SCHEME 7.29**   An example of alkane elimination in the synthesis of organouranium pincer complexes **83** and **84**.

Wilson et al. [95] have explored uranium and thorium chemistry of the related diamidoamine ligand $NN_2$ ($NN_2 = [Me_3SiN(CH_2CH_2NSiMe_3)_2]$). This pincer scaffold is unusual in that it contains no aromatic rings, and is thus highly flexible. Accordingly, the $NN_2$ framework has exhibited propensity to bind to actinide metals in both meridional and facial binding modes. A series of uranium (IV) and thorium (IV) halide and diligand complexes ($[NN_2]AnCl_2(THF)$, An = U, **85-U**; Th, **85-Th**, $[(NN_2)UCl_2]_2$, An = U, **86**, and $An[NN_2]_2$, An = U, **87-U**; Th, **87-Th**), potentially valuable as starting materials for subsequent chemistry, were synthesized by reaction of $AnCl_4$ and either 1 or 2 equivalents of $Li_2[NN_2]$ in THF. When $[NN_2]UCl_2(THF)$, **85-U**, was heated in toluene at 65°C, the THF molecule was lost, resulting in the chloride-bridged dimer $[(NN_2)UCl_2]_2$, **86-U** (Scheme 7.30) [95].
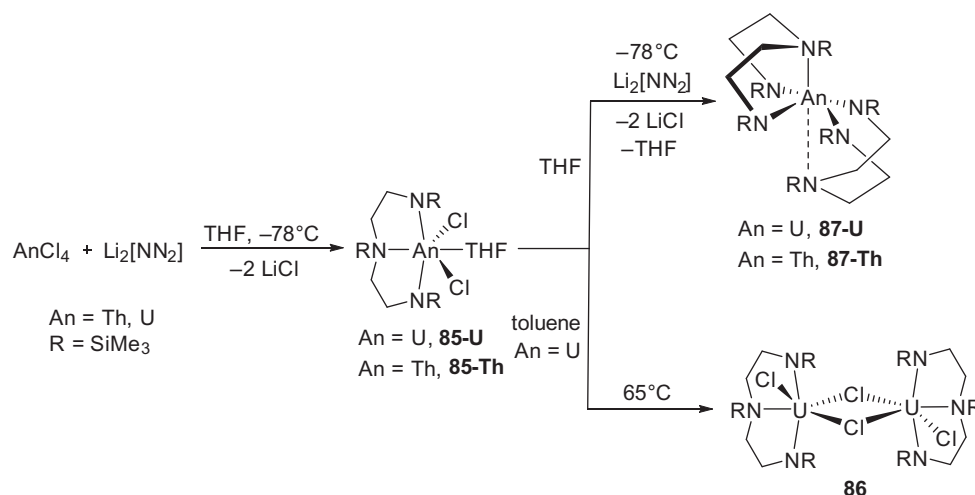
**SCHEME 7.30**  Synthesis of NNN pincer complexes **85–87**.

## 7.3.4  Trianionic Ligands

To our knowledge, the only example of a formal trianionic pincer ligand supporting an actinide metal was reported by Gambarotta and coworkers [96]. The dilithiated ligand $Li_2(THF)_4[1,3-(2,6-^iPr_2C_6H_3NC(=CH_2))_2C_6H_4]$ was combined with $UCl_4(THF)_4$ to give the uranium(IV) chloride "ate" complex, $Li(THF)_4[(1,3-(2,6-^iPr_2C_6H_3NC(=CH_2))_2C_6H_4)UCl_3]$, **88**. Notably, a noncovalent interaction between a phenyl C—H bond and uranium (U$\cdots$H = 2.5221 Å) was present in the X-ray crystal structure of the complex. Weakening of this C—H bond led to oxidative cleavage by addition of reducing K, forming the *NCN* trianionic ligated species $[1,3-(2,6-^iPr_2C_6H_3NC(=CH_2))_2C_6H_3]U(THF)(\mu\text{-}Cl)_2Li(THF)_2$, **89** (Scheme 7.31). Other attempts at generating reduced species led to solvent fragmentation products directed by a putative low-valent U(II) species.
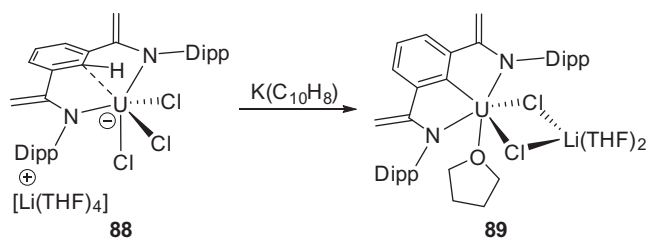


**SCHEME 7.31**  Synthesis of an unusual uranium complex supported by a trianionic *NCN* pincer ligand.

## 7.3.5  Redox-Active Ligands

This section focuses upon actinide complexes wherein the tridentate ligand scaffold supports redox activity, in that the ligand itself serves as the site of oxidation (L $\rightarrow$ L$^+$ + e$^-$) or reduction (L + e$^-$ $\rightarrow$ L$^-$). Many distinctions have been made regarding the nature of ligand redox activity; on one hand, the ligand radical can react with a substrate (actor), while spectator ligand types exert an effect on the central metal ion (spectator) (Fig. 7.6). The latter of these two
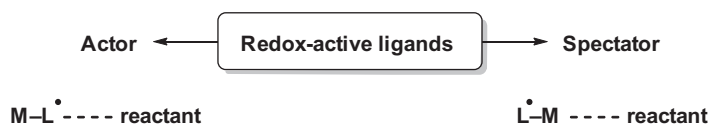


**FIGURE 7.6**  Classifications of redox-active ligands.

systems can be used as a temporary reservoir for electrons, with the metal as the locus of reactivity. Taken together, these ligands have enabled new chemistry not typically available for metals outside the platinum group. Uranium specifically is known to accommodate single-electron transformations. By combining a redox-active ligand capable of electron storage (spectator), noble metal reactivity can be conferred on the 5$f$ metal in bond activations, oxidative additions, and reductive transformations. It is important to note that we make no attempt to comprehensively review redox-active ligands, which is a rapidly growing field in organometallic, inorganic, and bioinorganic chemistry, and encompasses a variety of ligand scaffolds beyond the pincer class [97,98]. This discussion, rather, attempts to be as complete as possible within the context of actinide pincer chemistry. We purposefully avoid the term "noninnocent" in this chapter, given that physical oxidation states have been established using an array of techniques, including X-ray crystallography. Exhaustive efforts have been made by research groups to catalogue a sufficient quantity of data to compare and contrast intraligand bonding parameters, establishing "metrical oxidation states" (MOS) wherein the extent of oxidation at the metal center can be determined [99].

Redox activity with uranium is pertinent to this topic, given that the range of accessible oxidation states for the metal (III−VI) pair well with ligand redox events. By harnessing the electron mobility between uranium and the extended π-system of some pincer ligands, a variety of transformations have been achieved with a single metal-containing complex. Suzanne Bart has championed this area, particularly with respect to discrete electron transport from complexes of U(IV) ligated by highly reduced pincer frameworks. Such species have proven capable of performing challenging bond-breaking transformations. For example, multielectron shuttling from redox-active pincer complexes can result in the reductive cleavage of strong $N=N$ and $C=O$ double bonds in azobenzene and carbonyl derivatives [100,101].

### 7.3.5.1 Pyridine(diimine)

The most widely studied pincer ligand in the realm of redox-active actinide chemistry is the 2,6-pyridine(diimine) (PDI or bis(imino)pyridine) scaffold, which bears an entirely $N$-donor set (Scheme 7.32). From a practical standpoint, the family of PDI ligands allows for facile steric and electronic tuning through derivatization at multiple sites. Synthetically, variants of PDI are easily assembled from Schiff base condensation reactions between 2 equivalents of the desired aniline and the appropriately decorated 2,6-diacetylpyridine [102]. Notably, PDI ligands have been heavily studied for quite some time, with pioneering work by Brookhart and coworkers [102] and Gibson and coworkers [103] outlining its utility as a support for base metals (Fe, Co) in olefin polymerization catalysis. Since those initial reports, this $NNN$ pincer has become highly relevant across the periodic table [104,105].
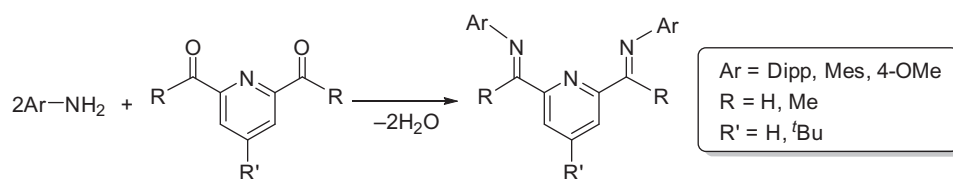


SCHEME 7.32 Common synthetic route to PDI ligands.

In a seminal contribution by de Bruin et al. in 2000 [106], the redox chemistry of diligand [$^{OMe}PDI^{Me}$]$_2$M complexes ($^{OMe}PDI^{Me}$ = 2,6-bis(1-(4-methoxyphenylimino)methyl)pyridine, M = Mn, Fe, Co, Ni, Cu, Zn) was discussed in depth. Chirik and Wieghardt [107] have since explained that PDI derivatives are stable across four oxidation levels (neutral, mono-, di-, and trianionic—[PDI]$^0$, [PDI]$^{1-}$, [PDI]$^{2-}$, [PDI]$^{3-}$). Hoyt et al. [108] have emphasized the pivotal role played by the [PDI]$^0$−[PDI]$^{2-}$ redox pair in the [2π + 2π] cycloisomerization of α,ω-dienes (Scheme 7.33). This result demonstrates that the PDI ligand can facilitate multielectron transfer while the oxidation state of the central metal remains constant throughout a catalytic cycle.

In actinide chemistry, the deliberate incorporation of functional multidentate ligands in place of carbocyclic derivatives has become a noticeable trend. The reducing nature of tri- and tetravalent uranium has been successfully combined with redox-active bidentate ligands to facilitate the 2-electron chemistry needed for bond formation and cleavage. Storage of additional electrons within an extended π-system allows for enhanced redox transformations, and partially
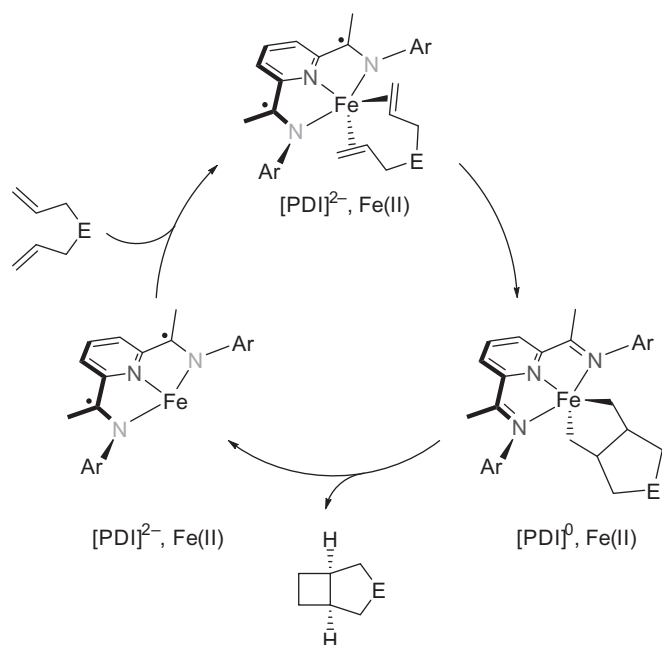
**SCHEME 7.33** Ring formation catalyzed by [PDI]Fe(II), during which the oxidation state of Fe is maintained throughout the catalysis; E = alkyl or nitrogen-substituted alkyl group; dark gray denotes neutral donors, light gray denotes anionic donors.

explains the slow departure from actinocene chemistry. This transition has been well represented by Suzanne Bart, who in 2013 introduced a two-component system containing $^{Mes}PDI^{Me}$ and Cp* ligands. Following that work, a series of reduced complexes were obtained by combining the neutral $[^{Mes}PDI^{Me}]^0$ ligand with trivalent Cp*UI$_2$(THF) and Cp$^P$UI$_2$(THF), promoting metal-based oxidation [U(III) → U(IV) + e$^-$] to give tetravalent uranium complexes ($[^{Mes}PDI^{Me}]^{1-}$UCp*I$_2$, **90-Cp\*** and $[^{Mes}PDI^{Me}]^{1-}$UCp$^P$I$_2$, **90-Cp$^P$** ($[^{Mes}PDI^{Me}]$ = 2,6-bis(1-(2,4,6-trimethylphenylimino) methyl)pyridine, Cp$^P$ = 1-(7,7-dimethylbenzyl)cyclopentadienyl)), with singly reduced pincer ligands (Schemes 7.34 and 7.35) [101]. Stepwise addition of intercalated graphite (KC$_8$) or Na[Et$_3$BH] promoted further ligand reduction ($[^{Mes}PDI^{Me}]^{2-}$UCp*I, **91-Cp\***, $[^{Mes}PDI^{Me}]^{2-}$UCp$^P$I, **91-Cp$^P$**, $[^{Mes}PDI^{Me}]^{3-}$UCp*(THF), **92-Cp\*** [109], $[^{Mes}PDI^{Me}]^{3-}$UCp$^P$, **92-Cp$^P$**) precipitating potassium or sodium iodide from the reaction mixture. Up to three electrons can typically be accommodated within the extended π-system of the PDI ligand [110].
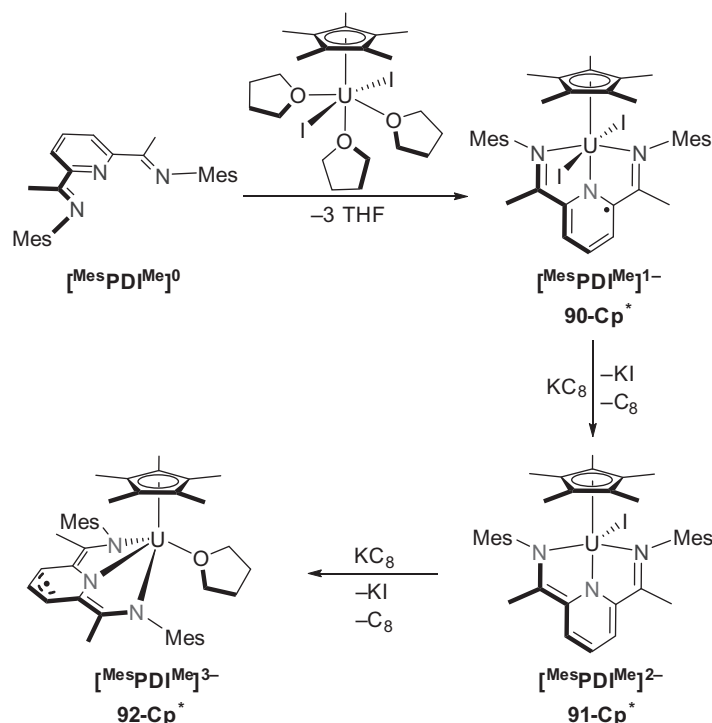


**SCHEME 7.34** Accessing mono-, di-, and trianionic PDI oxidation states in U(IV) complexes; dark gray denotes neutral donors, light gray denotes anionic donors.
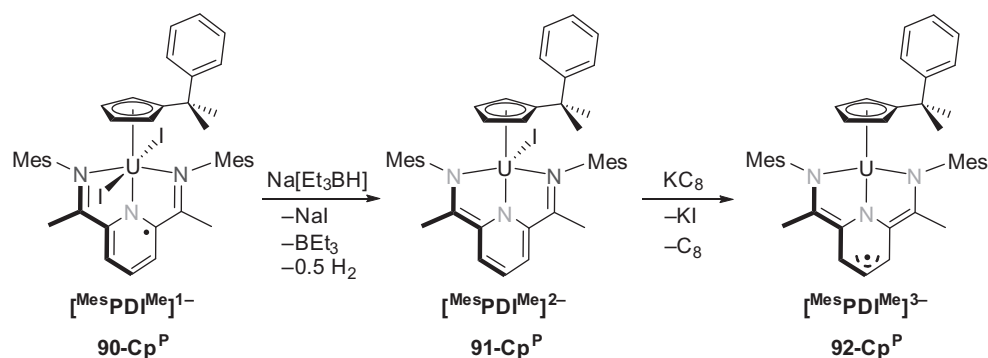
For these reduced derivatives, mono- and trianionic ligands are best described as $\pi$-radicals, with an odd electron count and spin state ($S = \frac{1}{2}$). The two electrons of the $[PDI]^{2-}$ ligand may spin-pair or remain in a triplet ground state. A suite of sophisticated techniques, most notably EPR spectroscopy and SQUID magnetometry, have aided in deconvoluting the complicated spin states of these systems [100,111]. DFT has also made significant contributions in understanding the bonding and reactivity in redox-active systems, and has been successfully applied to actinide redox chemistry. While this chapter does not attempt to cover the computational details of the referenced work, relevant results will be presented to aid the discussion; the interested reader is directed to the source material for additional details.

When comparing intraligand bond distances between high-valent uranium complexes and the free $[^{Mes}PDI^{Me}]^0$ ligand, evidence for localized ligand reduction can generally be obtained through X-ray crystallography. Recognizing the inherent challenges of assigning formal oxidation states in redox-active complexes, research groups have largely adopted the quantitative "MOS" [99]. This approach is based upon the concept that assessment of intraligand bond lengths within a complex, when compared to literature values for the free ligand, can be used to assign a formal oxidation state for the given ligand framework, and by association, the metal. PDI ligands further facilitate the study of discrete redox events by largely constraining high-valent metals to specific geometries. Redox events within the actinide pincer complex translate into subtle, but diagnostic, changes in bonding that can be observed crystallographically. For example, a survey of the 25 accessible PDI complexes of uranium in the Cambridge Structural Database (CSD) provided a $C = N_{imine}$ bond-distance range from 1.24 to 1.46 Å. This range accounts for PDI ligands in all available oxidation states ($0$, $1-$, $2-$, $3-$, and $4-$). Elongation of $C = N_{imine}$ bond lengths are the most pronounced in $PDI^{2-}$, $PDI^{3-}$, and $PDI^{4-}$ structures. To illustrate this matter, take the doubly reduced $[^{Mes}PDI^{Me}]^{2-}$ uranium complex $[^{Mes}PDI^{Me}]^{2-}UCp^*I$, **91-Cp\***, described by Bart and coworkers; iminic $C = N$ bond lengths (C2–N1) were significantly elongated compared to the diamagnetic $[^{Mes}PDI^{Me}]^0$ ligand [1.277(3) Å → 1.46(1) Å, i.e., $C = N_{imine}$ → $C-N_{enamine}$] (Fig. 7.7; Table 7.1) [101]. This parameter was the longest recorded in the CSD survey. Reduced PDI ligands in dimeric structures also exhibit long C–N bonds, though the steric pressure imposed through dimerization might play a role. Moreover, the adjacent C–C bond joining the imine donor to the central pyridine ring shortens significantly upon reduction. For example, in the same complex reported by Bart, contractions of this nature (C2–C3) indicated strong enaminic character (C = C) [1.495(3) Å → 1.39(1) Å, i.e., $C-C → C = C$] suggesting the locus of reduction is indeed the imine functionality. These data significantly alter the bonding picture within the complex, implying a shift from a neutral (dative) N→U interaction, to an anionic N–U bond for one of the two imine groups. When compared to the accompanying imine donor in the same $[^{Mes}PDI^{Me}]^{2-}$ complex (**91-Cp\***), minimal C–N bond lengthening (C8–N3)
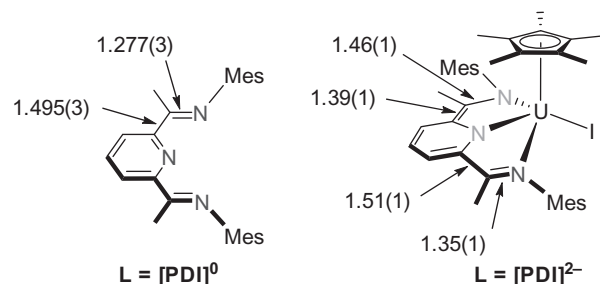


**FIGURE 7.7** Comparison of PDI bond lengths upon ligand reduction; dark gray denotes neutral donors, light gray denotes anionic donors.

**TABLE 7.1** Selected Bond Distances (Å) and Bond Angles (°) in 90-Cp$^P$, 91-Cp$^P$, 91-Cp*, and 92-Cp*

| Bond Lengths (Å) | | | | | |
|---|---|---|---|---|---|
| Parameter | [PDI]$^0$ | 90-Cp$^P$ [PDI]$^{1-}$ | 91-Cp$^P$ [PDI]$^{2-}$ | 91-Cp* [PDI]$^{2-}$ | 92-Cp* [PDI]$^{3-}$ |
| N1−C2 | 1.277(3) | 1.33(2) | 1.317(4) | 1.46(1) | 1.415(4) |
| C2−C3 | 1.495(3) | 1.48(2) | 1.441(4) | 1.39(1) | 1.359(5) |
| C3−C4 | 1.386(3) | 1.33(2) | 1.357(5) | 1.51(1) | 1.475(4) |
| C4−C5 | 1.378(3) | 1.38(2) | 1.404(5) | 1.35(1) | 1.423(5) |
| C5−C6 | 1.383(3) | 1.39(2) | 1.354(5) | 1.38(1) | 1.381(5) |
| C6−C7 | 1.388(3) | 1.39(2) | 1.416(5) | 1.43(1) | 1.488(4) |
| N2−C3 | 1.346(2) | 1.41(2) | 1.409(4) | 1.38(1) | 1.412(4) |
| N2−C7 | 1.343(3) | 1.39(1) | 1.427(4) | 1.36(1) | 1.392(4) |
| C7−C8 | 1.494(3) | 1.43(2) | 1.378(5) | 1.50(1) | 1.370(4) |
| N3−C8 | 1.276(3) | 1.33(1) | 1.375(4) | 1.35(1) | 1.407(4) |
| U−N1 | − | 2.52(1) | 2.500(2) | 2.156(8) | 2.300(3) |
| U−N2 | − | 2.37(1) | 2.234(3) | 2.337(8) | 2.203(2) |
| U−N3 | − | 2.484(9) | 2.327(3) | 2.781(8) | 2.315(2) |
| Bond Angles (°) | | | | | |
| N1−U−N2 | − | 67.2(4) | 65.35(9) | 73.8(3) | 72.12(9) |
| N2−U−N3 | − | 65.9(3) | 69.5(1) | 60.1(2) | 70.96(9) |
| N1−U−N3 | − | 133.2(3) | 127.92(9) | 117.9(3) | 122.65(9) |

was observed between the complex and the free ligand [1.35(1) vs 1.276(3) Å], while adjacent C−C lengths (C7−C8) are equivalent within error [1.494(3) vs 1.50(1) Å] (Table 7.1) [101].

In recognizing that data describing heavier atom connectivity is more accurate upon refinement, U−N distances have also served as a reliable metric to assess the oxidation state of both the metal and ligand. In closely related systems, complexes bearing the less sterically demanding Cp$^P$ (**90-Cp$^P$** and **91-Cp$^P$**), exhibited localized ligand reduction by X-ray crystallography [101]. Long U−N bonds were observed for neutral imine donors, whereas shortened U−N distances indicated a monoanionic uranium−amide bond. The dative interaction was identified in both imine fragments of complex **90-Cp$^P$**, where U−N1 = 2.52(1) Å and U−N3 = 2.484(9) Å. Reduction of **90-Cp$^P$** with KC$_8$ resulted in contraction of U−N3 to 2.327(3) Å while the change in U−N1 was insignificant [2.52(1) Å → 2.500(2) Å] (Table 7.1). This data provides a clear representation of the bonding between $^{Mes}$PDI$^{Me}$ and uranium; imine reduction occurred at one site, providing an overall dianionic ligand with both imine and amide N-donors.

Remarkably, in 2015, Bart et al. [112] provided compelling evidence for a tetraanionic PDI ligand within a dimeric uranium complex, thus redefining the extent to which the PDI framework can accommodate reducing equivalents. While the redox chemistry of PDI is operative in many transition metal-catalyzed reactions, combining the oxidizing capacity of the ligand with actinide metals and reducing agents has yielded interesting results that are thus far unparalleled in the transition metal domain. The complex of interest, [($^{Mes}$PDI$^{Me}$)$^{4-}$U(THF)]$_2$, **93**, was prepared by well-established methods in the Bart group: reduction of dimeric [($^{Mes}$PDI$^{Me}$)$^{3-}$UI]$_2$, **94** (which can be generated via double reduction of ($^{Mes}$PDI$^{Me}$)$^{1-}$UI$_3$(THF), **95**, or single reduction of ($^{Mes}$PDI$^{Me}$)$^{2-}$UI$_2$(THF)$_2$, **96**), with intercalated graphite to yield dimeric [($^{Mes}$PDI$^{Me}$)$^{4-}$U(THF)]$_2$, **93** (Scheme 7.36) [112,113]. Notably, this finding brings the total number of PDI ligand oxidation states to five. The authors concede that X-ray crystallography (Fig. 7.8) does not provide definitive evidence to clearly assign ligand oxidation state, particularly when one considers the steric hindrance of the dinuclear complex **93**, which certainly influences the structural parameters, perhaps in unexpected ways. However, the reducing nature of trivalent uranium renders a trianionic [$^{Mes}$PDI$^{Me}$]$^{3-}$ ligand representation rather unlikely.

**FIGURE 7.8** X-ray crystal structure of complex **93**; thermal ellipsoids drawn at 30% probability level, H-atoms and Dipp groups omitted for clarity,$' = -x, -y, -z$.

A ground-state electronic configuration of $5f^2$ was provided for both dimeric species **93** and **94**, backed up by XAS and computational (DFT) experiments. Variable-temperature magnetic data provided a singlet ground state for $[(^{Mes}PDI^{Me})^{4-}U(THF)]_2$, **93**, whereby ligand reduction has taken place, but electrons are paired, leaving the uranium (IV) center as the source of paramagnetism. Stability was supposedly achieved in the overall neutral $U_2N_2$ core through significant $\eta^5$-pyridine interactions between the reduced six-membered rings and the uranium centers, highlighting the significance of arene–actinide interactions (Fig. 7.8). Interaction energies (PBE/ZORA/STO-TZ2P level) showed that $[(^{Mes}PDI^{Me})^{4-}U(THF)]_2$ is more stable than $(^{Mes}PDI^{Me})^{3-}UI]_2$, **94**, by 23.3 kcal/mol, a result of additional $\delta$ back bonding in the former complex [112]. Experimentally, the stability conferred by arene interactions is manifested in the prolonged shelf-life of $[(^{Mes}PDI^{Me})^{4-}U(THF)]_2$ in the solid state (multiple days), whereas $[(^{Mes}PDI^{Me})UI]_2$ decomposes after several hours under the same conditions [112].

The redox reactivity of the electron-rich dimers **93** and **94** had been previously highlighted in the reduction of $N_3Mes$, generating bis- and tris(imido) products with neutral $^{Mes}PDI^{Me}$ ligands, along with dinitrogen from the organoazide [113]. These multielectron processes were complemented by single redox events, specifically the 1-electron oxidation of $[(^{Mes}PDI^{Me})^{4-}U(THF)]_2$ back to $[(^{Mes}PDI^{Me})^{3-}UI]_2$ using 1 equivalent of $I_2$ [112]. Further addition of $I_2$ or CuI eventually regenerated $[^{Mes}PDI^{Me}]^{1-}UI_3(THF)$, **95** (Scheme 7.36). The reductive potency of the reduced dimers was harnessed in a display of comproportionation reactivity (Scheme 7.37). Combining $[(^{Mes}PDI^{Me})^{4-}U(THF)]_2$ with $[^{Mes}PDI^{Me}]^{2-}UI_2(THF)_2$ afforded $[(^{Mes}PDI^{Me})^{3-}UI]_2$ in quantitative yield, which when combined with $[^{Mes}PDI^{Me}]^{1-}UI_3(THF)$ gave $[^{Mes}PDI^{Me}]^{2-}UI_2(THF)_2$ [112]. These single-electron redox reactions show promise in fundamental transformations, adding to established multielectron transfer reactivity demonstrated by actinide complexes of PDI. The reductive capacity of the PDI framework is well established for transition metals, and now that Bart has bridged the gap to include actinide metals, an increasingly complex collection of organometallic and inorganic chemistry is expected to be uncovered.
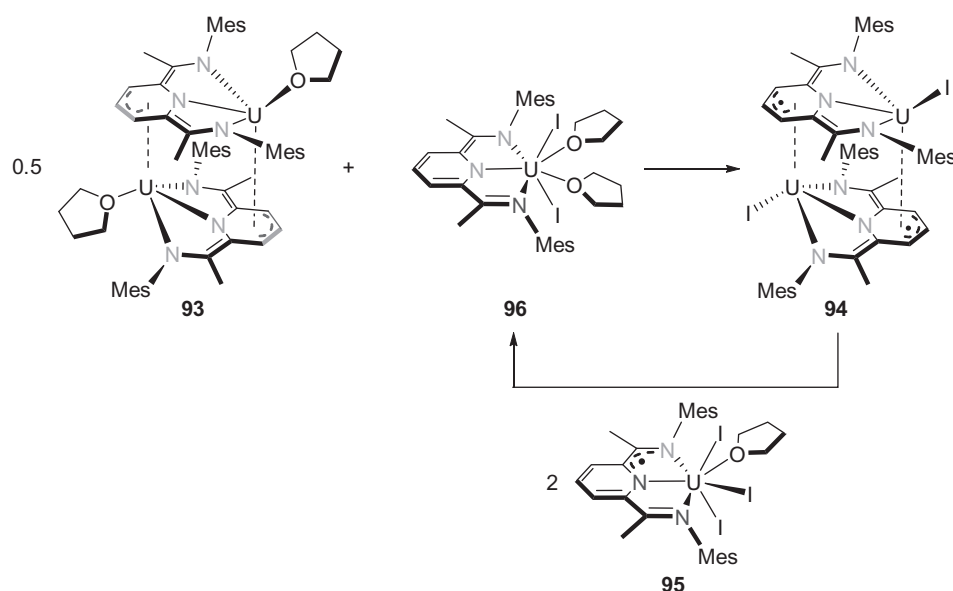


**SCHEME 7.37** Comproportionation reactions showcasing reductive potency of complexes **93** and **94**; dark gray denotes neutral donors, light gray denotes anionic donors.

### 7.3.5.2 Dioxophenoxazine

As described in the previous section, the majority of work in the growing field of actinide pincer redox activity involves derivatives of the bis(imino)pyridine (PDI) ligand. Nevertheless, new classes of ligands are emerging, in particular the rigid dioxophenoxazine (DOPO) family (2,4,6,8-tetrakis(tert-butyl)-9-hydroxy-1H-phenoxazin-1-one), which has demonstrated stability as mono-, di-, and trianionic *NON* ancillary ligands (Fig. 7.9). The redox chemistry of actinide DOPO complexes developed in much the same way as the PDI-supported species, in that early work focused on diligand metal complexes of the first-row transition series [98,106]. In fact, both such publications describe redox chemistry of the respective ligand with the same six metals: Mn, Fe, Co, Ni, Cu, Zn [106,114]. Later reports assessed the electronic structure of reduced DOPO ligands with Cr, Mo, W [115]. Following similar protocols that provided PDI
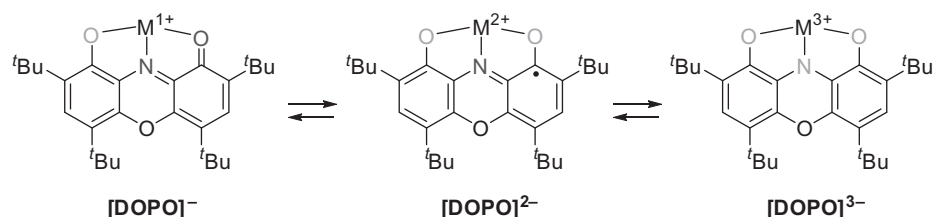


**FIGURE 7.9** Accessible oxidation states of DOPO ligands; dark gray denotes neutral donors, light denotes anionic donors.

actinide complexes, uranium iodide species $[DOPO]^{2-}UI_2(THF)_2$, **97**, and $[DOPO]^{3-}UI(THF)_2$, **98**, were generated through salt metathesis reactions between potassiated DOPO ligand and $U(I)_3(THF)_4$ (Scheme 7.38) [116]. Notably, metal-to-ligand electron transfer provided a planar dianionic $[DOPO]^{2-}$ ligand (complex **97**), which exhibited semiquinone character, wherein the MOS of the ligand was $2-$. These data confirm complex **97** is neutral with uranium in the $4+$ oxidation state; two iodide ligands and two THF molecules fill the remaining coordination sites [116].
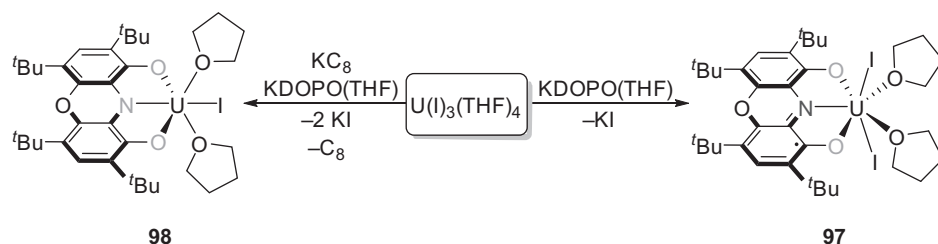


**SCHEME 7.38** Synthetic routes to uranium(IV) complexes of a DOPO ligand; dark gray denotes neutral donors, light gray denotes anionic donors.

By virtue of its relatively rigid ether linkage, the extended π-system in DOPO is constrained to be quite planar. This planarity increases electron storage capacity compared to 3,5-di-tert-butyl-1,2-quinone-1-(2-oxy-3,5-di-tert-butylphenyl) imine (ONO) frameworks (Chart 7.4) [117]. It should be noted that planarity in ONO scaffolds is typically only achieved with the addition of chelating *ortho*-quinone ligands, which share unpaired electron density. Since DOPO ligands generally maintain planarity, assignment of MOS (*vide supra*), and hence identification of the locus of reduction/oxidation, tends to be straightforward.
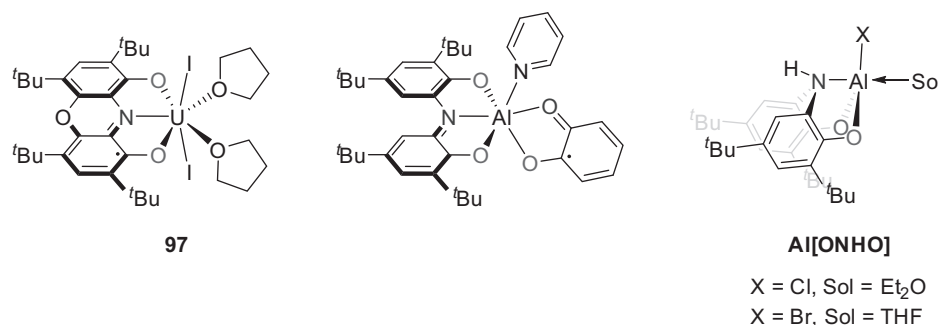


**CHART 7.4** Examples of $DOPO^{2-}$ and $ONO^{2-}$ complexes; dark gray denotes neutral donors, light gray denotes anionic donors.

### 7.3.5.3 Terpy: 2,2′:6′,2″-terpyridine

In differentiating between reactive metals from the lanthanide and actinide series, multidentate *N*-heterocyclic ligands have contributed significantly to the understanding of how 4*f* and 5*f* electrons participate in metal−ligand bonding. Beyond a fundamental understanding of bonding in *f*-elements, research in this area has contributed to advances in the sequestration of nuclear waste products by the selective complexation of *NNN* pincer ligands to trivalent actinides [19,37,38]. While discrepancies between lanthanide and actinide complexes of the form $[Cp*_2M(L)]^{n+}$ have been reported (M = Ce, U; L = 2,2′-bipyridine (bipy), 1,10-phenanthroline (phen)), the most pronounced differences occur within the pincer context. Specifically, trivalent cerium and uranium complexes of the *NNN* pincer terpy, have demonstrated redox activity. Recognizing that electron donation into the LUMO of the neutral *N*-heterocyclic bipy ligand was greater for the actinide complex Cp*_2UI(bipy) than for its lanthanide analogue [Cp*_2CeI(bipy), terdentate ligands with an extended π-system presented a logical next step in understanding such interactions. Thus, in the same report, Ephritikhine and coworkers [39] conducted a comparative study of the neutral complexes $[terpy]^{1-}MCp*_2$ (M = U, **99-U**; Ce, **99-Ce**). These complexes were prepared in high yield (92% for Ce, 90% for U) by facile reduction of the cationic precursors $[(terpy)^0MCp*_2][I]$ (M = U, **100-U**; Ce, **100-Ce**) (Scheme 7.39).
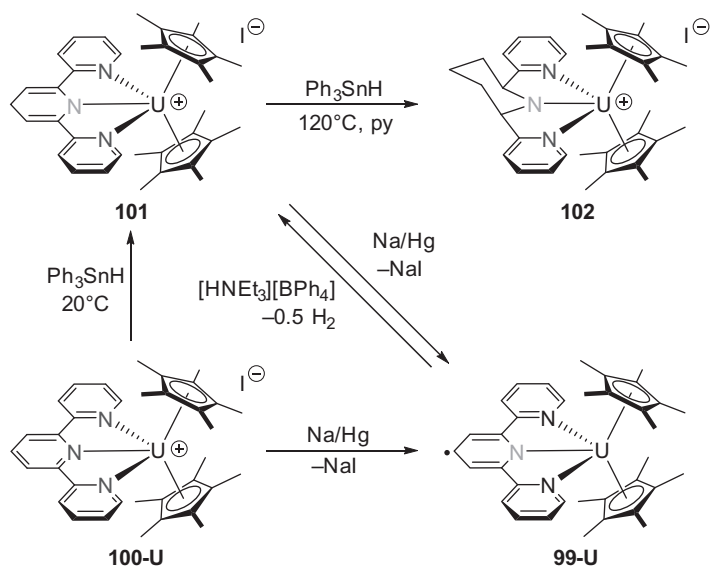
**SCHEME 7.39** Reaction chemistry of actinocene terpy complexes; dark gray denotes neutral donors, light denotes anionic donors.

Careful examination of the structural parameters in the cationic precursors **100** revealed systemic contractions in U−N, relative to Ce−N bond distances. Extensive electron donation from the UCp*$_2$ core into the LUMO of the neutral terpy ligand in complex **100-U** supported these observations, and would eventually lead to metal-based oxidation [U(III)→U(IV) + e$^-$]. Canonical representations of the complexes have been provided (Chart 7.5); for the cationic cerium(III) complex, the diamagnetic terpy ligand (A) is the major contributor, whereas for the analogous cationic uranium(III) complex the terpy ligand bears unpaired spin density (B−D). Radical ligand character (E) is present in the neutral complexes **99-Ce** and **99-U**, but the extent of electron mobility is more dramatic in the uranium complex, wherein an ion-pair representation (F) best describes the system. Magnetic studies of [terpy]$^{1-}$MCp*$_2$ established that the ligand is a radical anion (terpy$^-$) which couples antiferromagnetically to the metal at low temperatures (<5 K). For complex **99-U**, this was the first instance where magnetic exchange between uranium(III) and a spin carrier was observed in a molecular complex [39].
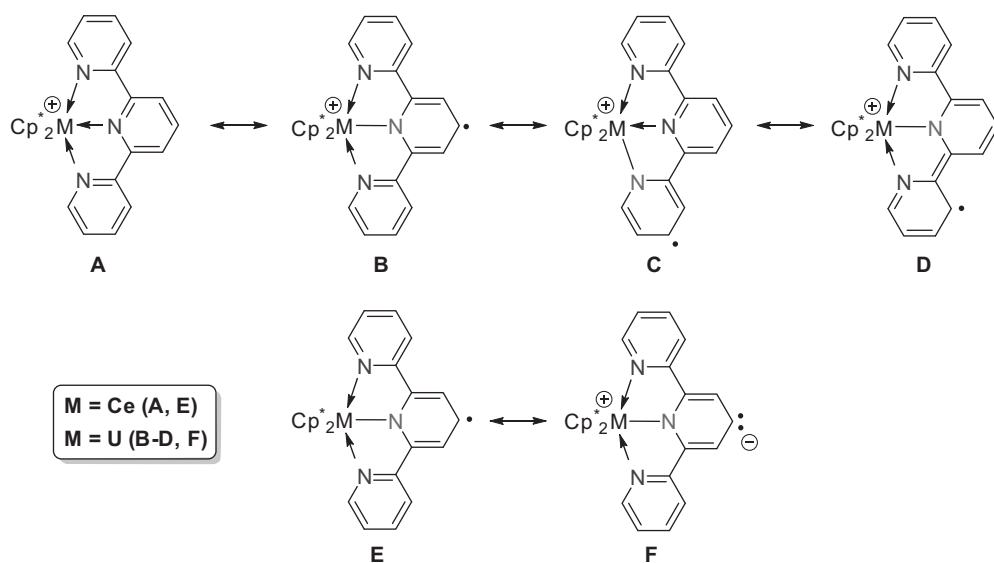


**CHART 7.5** Redox contributors for uranium and cerium terpy complexes; dark gray denotes neutral donors, light gray denotes anionic donors.

The difference between cerium and actinide pincer complexes is perhaps best illustrated in their reactivity profiles with the H· and H$^+$ donors Ph$_3$SnH and [HNEt$_3$][BPh$_4$]. Complex **100-Ce** [(terpy)$^0$CeCp*$_2$][I] did not react with Ph$_3$SnH or [HNEt$_3$][BPh$_4$]. This inertness stands in sharp contrast to **100-U** [(terpy)$^0$UCp*$_2$][I], which upon combination with Ph$_3$SnH at 20°C afforded [(terpyH)$^{1-}$U Cp*$_2$][I], **101**, the product of hydrogen atom transfer (HAT) (Scheme 7.35) [39]. The central monohydroterpyridyl (2,6-dipyridyl(hydro-4-pyridyl) unit was the first of its kind, and was characterized by X-ray crystallography; the length between uranium and the central nitrogen atom (2.313(6) Å) in **101**, when compared to 2.419(5) Å in **100-U**, suggests conversion from a neutral pyridine donor to a monoanionic amide. A drastic change in the central ring was observed upon complete hydrogenation with excess Ph$_3$SnH in refluxing pyridine. Specifically, the piperidinyl donor in [(terpyH$_5$)$^{1-}$U Cp*$_2$][I], **102**, adopts a chair conformation in the solid state, with further contraction of the central U−N contact to 2.247(7) Å.

Reduction of complex **101** with sodium amalgam generated **99-U**. Addition of the proton source [HNEt$_3$][BPh$_4$] to **99-U** reversed the reaction to regenerate **101**, along with concomitant production of 0.5 equivalent of H$_2$ [39]. These crystallographic data and reactivity profiles demonstrate the enhanced electron mobility within actinide pincer complexes of the terpy ligand.

### 7.3.5.4 Bond Activation by Redox-Active Actinide Pincer Complexes

Capitalizing on the extent to which the PDI ligand can host reducing equivalents, and drawing inspiration from Evans' 4-electron reduction chemistry with U(III) [15], Bart and coworkers sought to achieve productive multielectron reactivity with the uranium(IV) complex [$^{Mes}$PDI$^{Me}$]$^{3-}$UCp*(THF), **92-Cp*** [112]. Remarkably, the three electrons stored in the pincer ligand combined with one electron from uranium(IV) to affect the 4-electron reduction of azobenzene and give the uranium(V) bis(imido) complex [$^{Me}$PDI$^{Mes}$]$^0$UCp*(NPh)$_2$, **103** (Scheme 7.40) [109]. From the structural parameters obtained by X-ray crystallography, the diamagnetic [$^{Mes}$PDI$^{Me}$]$^0$ ligand was strongly implicated. For example, the coplanar arrangement of the N atoms in the ligand was restored and all signs of C−N bond reduction were lost. The ambient temperature (23°C) magnetic moment for complex **103** is 1.75(1) $\mu_B$, which is consistent with pentavalent uranium. Thus, complex **103** is best described as a U(V) center bearing a neutral pincer, two NPh$^{2-}$ donors, and one C$_5$Me$_5$$^-$ ligand. At the time of the original publication, the X-ray crystal structure of the neutral [$^{Mes}$PDI$^{Me}$]$^0$ ligand was not available to draw meaningful comparisons of intraligand bonding; we have provided these data in Table 7.2.
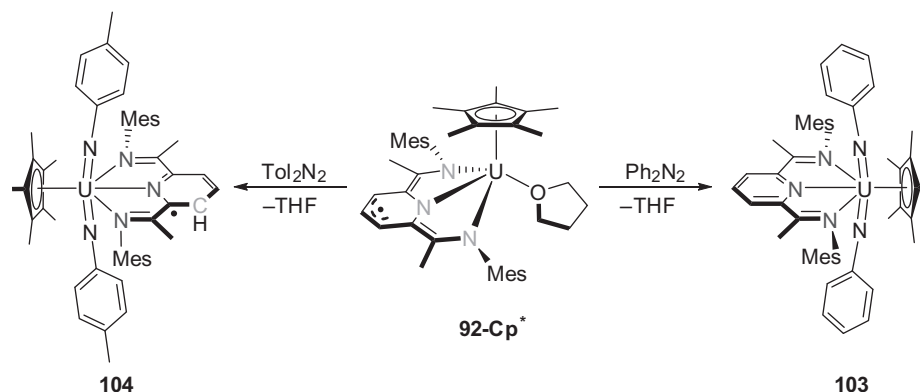


**SCHEME 7.40** Reductive cleavage of azobenzenes by [$^{Mes}$PDI$^{Me}$]$^{3-}$UCp*(THF), **92-Cp***; dark gray denotes neutral donors, light gray denotes anionic donors.

**92-Cp***

**104**

**103**

Altogether, the aforementioned information corroborates the presence of a neutral ligand. Most significantly, the redox-active ligand has been retained at the metal and not sacrificed, as has been the case in the previous work; the chelating nature of pincer ligands is advantageous in this respect. In a later study, Bart et al. [110] described the effect of substitution at the imide donor. Notably, by changing the aryl group on the imide to the more electron donating *p*-tolyl, the high-valent U(VI) species [$^{Me}$PDI$^{Mes}$]$^{1-}$UCp*(N(4-MeC$_6$H$_4$))$_2$ [110], **104**, prevailed. The buildup of electron density on the meta-carbon of the pyridine ring resulted in a ligand-centered radical anion (Scheme 7.40). It is important to note that the assignments of U(V) and U(VI) oxidation states were corroborated by XAS. Since the initial report in 2013, this multielectron chemistry has been harnessed in the preparation of mono-, bis-, and through the reduction of organoazide, tris(imido) complexes [100,110,113].

**TABLE 7.2** Selected Bond Distances (Å) in [$^{Mes}PDI^{Me}$]$^0$ and [$^{Me}PDI^{Mes}$]$^0UCp^*(NPh)_2$, 103

| Parameter (Å) | [$^{Mes}PDI^{Me}$]$^0$ | [$^{Me}PDI^{Mes}$]$^0UCp^*(NPh)_2$ (103) |
|---|---|---|
| N1−C2 | 1.277(3) | 1.290(8) |
| C2−C3 | 1.495(3) | 1.495(9) |
| C3−C4 | 1.386(3) | 1.376(9) |
| C4−C5 | 1.378(3) | 1.39(1) |
| C5−C6 | 1.383(3) | 1.38(1) |
| C6−C7 | 1.388(3) | 1.380(9) |
| N2−C3 | 1.346(2) | 1.348(8) |
| N2−C7 | 1.343(3) | 1.350(8) |
| C7−C8 | 1.494(3) | 1.480(8) |
| N3−C8 | 1.276(3) | 1.295(8) |

In exploring the reductive capacity of PDI, bond formation and activation of carbonylated substrates were targeted by Bart et al. [101]. Combining the partially reduced **91-Cp*** with furfural ($C_5H_4O_2$) promoted the 1-electron oxidation of the ligand. Radical coupling between the putative cationic intermediate [($^{Mes}PDI^{Me}$)UCp*]$^+$ and the ketyl anion was corroborated by X-ray crystallography, which revealed alkoxy-amide $^{Mes}PDI^{Me}$ ligands in [$^{Me}PDI^{Mes}$]$^{1-}$UCp*I(OCH($C_4H_3O$)), **105** (Scheme 7.41).
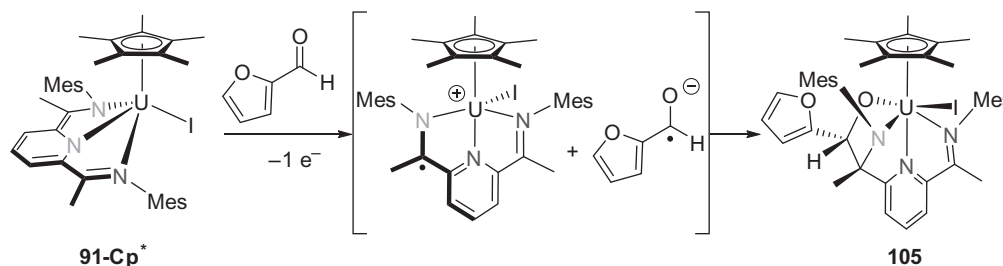


**SCHEME 7.41**    Reductive coupling of CO to a PDI ligand; dark gray denotes neutral donors, light gray denotes anionic donors.

Viable carbonylated substrates for this coupling scheme were defined, but the reactivity of benzophenone and acetophenone differed from that of furfural. Substrate coupling was identified by X-ray crystallography, as well as spectroscopic data (IR) that indicated the disappearance (reduction) of CO [101]. The steric influence of the carbocyclic ligand was crucial in the reactivity profiles for the carbonyl substrates. The Cp* and Cp$^P$ complexes were selected for radical C−C coupling of the carbonyl substrates, targeting pinacolate complexes of uranium. The presence of the sterically demanding Cp* precluded coupling of benzophenone (2 equivalents); however, when the smaller acetophenone substrate was employed, the uranium *meso*-pinacolate [$^{Me}PDI^{Mes}$]$^{1-}$UCp*I($O_2C_2Ph_2H_2$), **106**, was generated. Perhaps unsurprisingly, 2 equivalents of benzophenone readily combined in the less bulky **92-Cp$^P$**, giving pinacolate [$^{Me}PDI^{Mes}$]$^{1-}$UCp*I($O_2C_2Ph_4$), **107** [101]. The reductive schemes presented in Scheme 7.42 highlight the promise of this strategy has for the activation of a variety of small molecules.
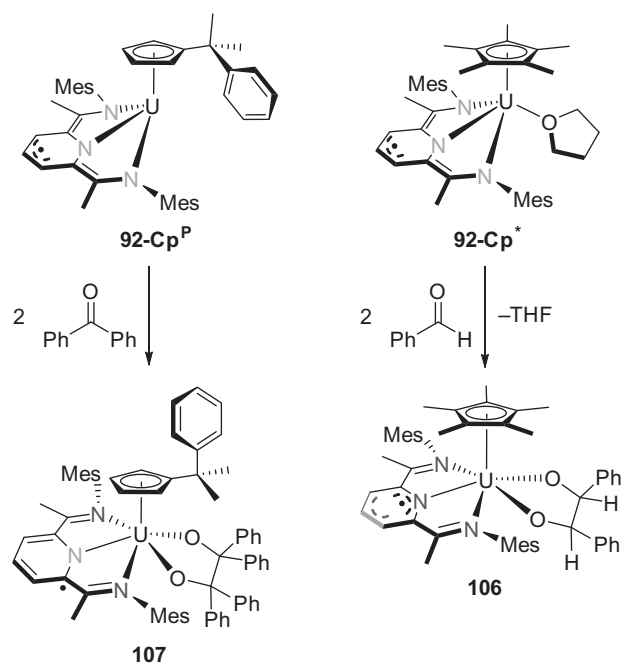
**SCHEME 7.42** Reductive coupling of ketones and aldehydes; dark gray denotes neutral donors, light gray denotes anionic donors.

## 7.4 CATALYTIC REACTIONS MEDIATED BY ACTINIDE PINCER COMPLEXES

While the development of actinide pincer complexes has accelerated immensely in recent years, examples of utilizing such species to catalyze chemical reactions remain scarce. Catalytic processes involving actinide metals often involve σ-bond metathesis pathways that proceed via a four-membered transition state [118]. By comparison, oxidative addition and reductive elimination pathways, while not unprecedented, are rare. Hence, similar catalytic processes to those mediated by rare earth metals tend to predominate. The most explored catalytic transformations invoking actinides are olefin polymerization, ring opening of cyclic esters, and hydroelementation (e.g., hydroamination, hydrosilation) reactions [119−121].

### 7.4.1 Hydroamination

Virtually all examples of actinide pincer-based catalysis have come from the Leznoff group, who have used their versatile actinide diamido-ether complexes to catalyze a variety of reactions. For example, a library of thorium(IV) and uranium(IV) halide and alkyl complexes (Chart 7.6) exhibited catalytic competence in the intramolecular hydroamination of aminoalkenes (Scheme 7.43) [122].
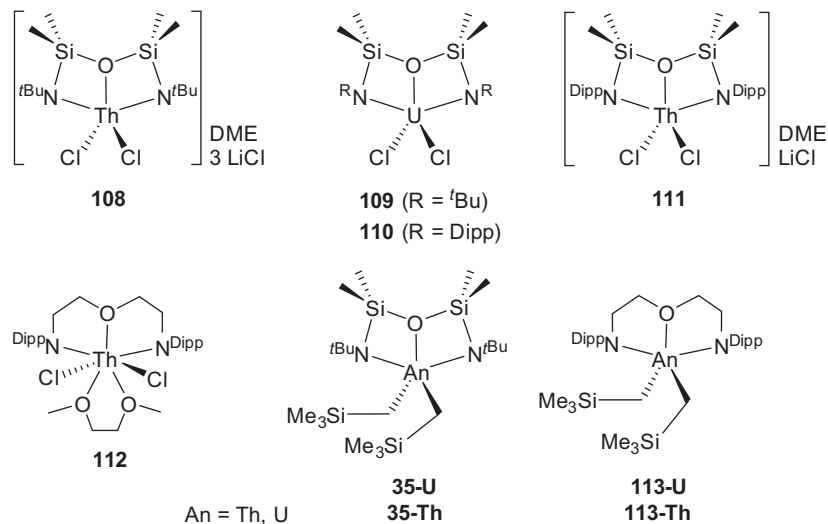


**CHART 7.6** Actinide pincer complexes that have exhibited activity as catalysts for intramolecular hydroamination.
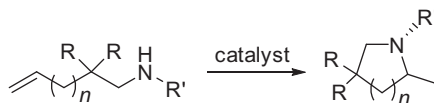
**SCHEME 7.43**    Example of intramolecular hydroamination catalyzed by actinide pincer complexes.

It was established that the thorium complexes were generally more active than their uranium analogues, a result that was attributed to the greater ionic radius of Th(IV) compared to U(IV) (Th(IV) = 1.09 Å cf. U(IV) = 1.05 Å). It was also determined that ligands with bulkier substituents on nitrogen promoted higher activity in most systems [122]. Complexes bearing chloride ligands showed varying activity toward intramolecular hydroamination, and the less rigid [$^{Dipp}$NCOCN] ligand ([$^{Dipp}$NCOCN] = {2,6-$^i$PrPhN(CH$_2$CH$_2$)}$_2$O) provided more catalytically active species than the *NON* family of ligands, [$^{tBu}$NON] and [$^{Dipp}$NON] ([$^{tBu}$NON] = (Me$_3$CNH(SiMe$_3$)$_2$)$_2$O, [$^{Dipp}$NON] = {2,6-$^i$PrPhN(SiMe$_2$)}$_2$O).

## 7.4.2    Ring-Opening Polymerization

Leznoff and coworkers [123] also explored the ring-opening polymerization of lactide (Scheme 7.44) catalyzed by diamidoether actinide complexes (Chart 7.7).
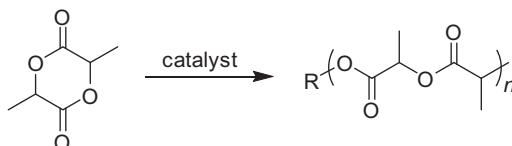


**SCHEME 7.44**    Ring-opening polymerization of lactide.

It was determined that all complexes studied were active initiators toward the polymerization of *L*-lactide under ambient conditions except [$^{Dipp}$NCOCN]U(CH$_2$SiMe$_3$)$_2$, **113-U**, which proved stubbornly inactive. The polydispersity [PDI, ($M_w$/$M_n$)] of the resulting polylactide polymers typically ranged from 1.1 to 1.6, with complete consumption of 50 equivalents of monomer generally observed in 1 h or less. Contrary to the aforementioned hydroamination, the activities of complexes bearing the *NON* ligand scaffolds were generally superior to those supported by the *NCOCN* framework. Analysis by NMR spectroscopy and MALDI-TOF mass spectrometry indicated that the alkyl and alkoxide functionalities were the sole initiating groups, and that the diamidoether ligand remains firmly bound to the metal (no evidence was found for polymers containing pincer end groups). Complex [$^{tBu}$NON]U(O$^i$Pr)$_2$, **114**, was shown to be the best initiator for ring-opening polymerization of lactide and was thus further explored in regard to *rac*-lactide polymerization. Notably, it displayed moderate preference for heterotactic linkages ($P_r$ = 0.73 in THF), presumably via a chain end control mechanism.
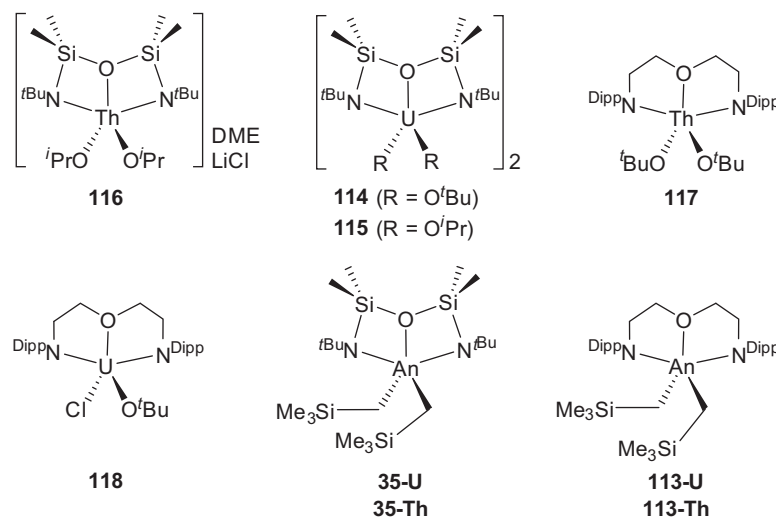


**CHART 7.7**    Actinide complexes based on *NON* pincer ligands screened for ROP catalysis.

### 7.4.3 Ethylene Polymerization

Finally, the Leznoff group explored the polymerization of ethylene using several U(IV) catalysts that feature similar diamidoether ligands and alkyl functionalities (Chart 7.8) [124]. One of the catalysts studied was an alkyl-bridged uranium dimer $[(^{tBu}NON)U\{CH(SiMe_3)(SiMe_2CH_2)\}]_2$, **119**, which formed via C−H bond activation of a $CH(SiMe_3)_2$ group. Reaction of these complexes under an atmosphere of ethylene produced high molecular weight polyethylene, but with relatively high PDIs. Generally, complexes featuring the *NON* ligand exhibited higher activity than those bearing the *NCOCN* ligand. Intriguingly, when typical Lewis acidic co-catalysts, such as $B(C_6F_5)_3$, $Et_2AlCl$ or MMAO were added, the activity of the catalyst was dramatically hindered or even deactivated altogether in some cases. Thus, these pincer complexes represent several of the scant few examples of single-component, actinide-based olefin polymerization catalysts.
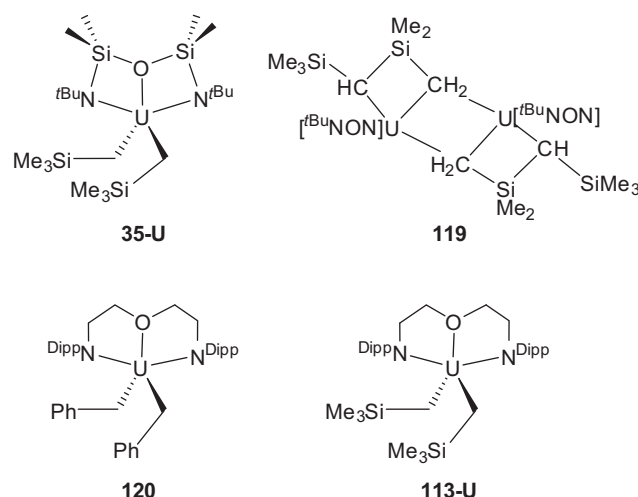


**CHART 7.8**  Actinide complexes based on *NON* pincer ligands screened for ethylene polymerization catalysis.

Despite the observed reactivity by Leznoff and coworkers, coordinatively unsaturated cationic complexes are typically far superior ethylene polymerization catalysts than their neutral counterparts. The high Lewis acidity of cationic complexes, however, can attract Lewis base or even arene coordination which can hinder catalytic activity. For example, the Emslie group reported remarkable cationic thorium complexes $[(XA_2)Th(\eta^1\text{-}CH_2Ph)][\eta^6\text{-}PhCH_2B(C_6F_5)_3]$, **24**, and $[(XA_2)Th(CH_2SiMe_3)(\eta^6\text{-arene})][B(C_6F_5)_4]$ (arene $= C_6H_6$, toluene), **26** [58], which proved to be inactive toward ethylene polymerization, due to tight arene coordination. Lewis base and arene-free cationic actinide complexes are difficult to isolate as they are often highly unstable, but evidently, coordination can hinder, or entirely shutter catalytic reactivity. As work continues to be done, and a better balance between chemical inertness and self-destruction becomes more accessible, the discovery of highly active and selective catalysts is inevitable.

## 7.5 CONCLUSION

In this chapter, the chemistry of actinide pincer complexes has been reviewed, highlighting the synthetic approaches taken, the inherent challenges of working with, and most crucially, the unique reactivity exhibited by 5*f* elements. A host of pincer ligands, some of which have served in a variety of transformations, including selective extraction from nuclear waste and as active participants in redox reactions, have been successfully paired with uranium and thorium. The field of actinide catalysis is in its infancy, and while the scope of catalysis remains somewhat limited, future work will undoubtedly lead to exciting discoveries.

### ACKNOWLEDGMENTS

## REFERENCES

[1] S.A. Cotton, Annual Reports Section "A" (Inorganic Chemistry) 106 (2010) 286.
[2] S. Cotton, Lanthanide and Actinide Chemistry, John Wiley & Sons, 2006, p. 145.
[3] F.T. Edelmann, Coord. Chem. Rev. 257 (2013) 1122.
[4] F.T. Edelmann, Coord. Chem. Rev. 318 (2016) 29.
[5] A. Yahia, L. Maron, Organometallics 28 (2009) 672.
[6] L. Castro, A. Yahia, L. Maron, Chem. Phys. Chem. 11 (2010) 990.
[7] R.M. Diamond, K. Street, G.T. Seaborg, J. Am. Chem. Soc. 76 (1954) 1461.
[8] J.N. Cross, J. Su, E.R. Batista, S.K. Cary, W.J. Evans, S.A. Kozimor, et al., J. Am. Chem. Soc. 139 (2017) 8667.
[9] L.J. Nugent, R.D. Baybarz, J.L. Burnett, J. Phys. Chem. 73 (1969) 1177.
[10] D.B. Leznoff, C.E. Hayes, G. Mund, Encyclopedia of Inorganic and Bioinorganic Chemistry, John Wiley & Sons:, 2011.
[11] C.E. Hayes, D.B. Leznoff, Coord. Chem. Rev. 266−267 (2014) 155.
[12] P.J. Fagan, J.M. Manriquez, T.J. Marks, In: T.J. Marks, R.D. Fischer (Eds.), Organometallics of the f-Elements: Proceedings of the NATO Advanced Study Institute held at Sogesta, Urbino, Italy, September 11−22, 1978, Springer, Dordrecht, The Netherlands, 1979, p. 113.
[13] T.J. Marks, J.R. Kolb, Chem. Rev. 77 (1977) 263.
[14] T.J. Marks, Progress in Inorganic Chemistry, John Wiley & Sons, Hoboken, NJ, 2007, p. 223.
[15] W.J. Evans, S.A. Kozimor, J.W. Ziller, Chem. Commun. (2005) 4681.
[16] W.J. Evans, S.A. Kozimor, J.W. Ziller, A.A. Fagin, M.N. Bochkarev, Inorg. Chem. 44 (2005) 3993.
[17] W.J. Evans, D.J. Wink, D.R. Stanley, Inorg. Chem. 21 (1982) 2565.
[18] J.-C. Berthet, J. Maynadié, P. Thuéry, M. Ephritikhine, Dalton Trans. 39 (2010) 6801.
[19] J.-C. Berthet, Y. Miquel, P.B. Iveson, M. Nierlich, P. Thuéry, C. Madic, et al., J. Chem. Soc., Dalton Trans. (2002) 3265.
[20] J.-C. Berthet, M. Nierlich, Y. Miquel, C. Madic, M. Ephritikhine, Dalton Trans. (2005) 369.
[21] J.-C. Berthet, C. Rivière, Y. Miquel, M. Nierlich, C. Madic, M. Ephritikhine, Eur. J. Inorg. Chem. 2002 (2002) 1439.
[22] J.R. Khusnutdinova, D. Milstein, Angew. Chem. Int. Ed. 54 (2015) 12236.
[23] D. Morales-Morales, C.M. Jensen, The Chemistry of Pincer Compounds, Elsevier Science B.V., Amsterdam, 2007.
[24] M.M. Hänninen, M.T. Zamora, P.G. Hayes, In: G. van Koten, R.A. Gossage (Eds.), The Privileged Pincer-Metal Platform: Coordination Chemistry & Applications, Springer International Publishing, Cham, Switzerland, 2016, p. 93.
[25] L.R. Avens, S.G. Bott, D.L. Clark, A.P. Sattelberger, J.G. Watkin, B.D. Zwick, Inorg. Chem. 33 (1994) 2248.
[26] C.D. Carmichael, N.A. Jones, P.L. Arnold, Inorg. Chem. 47 (2008) 8577.
[27] J.-C. Berthet, P. Thuéry, M. Ephritikhine, Inorg. Chem. 44 (2005) 1142.
[28] A.E. Enriquez, B.L. Scott, M.P. Neu, Inorg. Chem. 44 (2005) 7403.
[29] T. Cantat, B.L. Scott, J.L. Kiplinger, Chem. Commun. 46 (2010) 919.
[30] D.L. Clark, T.M. Frankcom, M.M. Miller, J.G. Watkin, Inorg. Chem. 31 (1992) 1628.
[31] N.E. Travia, M.J. Monreal, B.L. Scott, J.L. Kiplinger, Dalton Trans. 41 (2012) 14514.
[32] A.J. Gaunt, A.E. Enriquez, S.D. Reilly, B.L. Scott, M.P. Neu, Inorg. Chem. 47 (2008) 26.
[33] S.D. Reilly, J.L. Brown, B.L. Scott, A.J. Gaunt, Dalton Trans. 43 (2014) 1498.
[34] S.A. Johnson, J.J. Kiernicki, P.E. Fanwick, S.C. Bart, Organometallics 34 (2015) 2889.
[35] M.A. Boreen, B.F. Parker, T.D. Lohrey, J. Arnold, J. Am. Chem. Soc. 138 (2016) 15865.
[36] J.-C. Tourneux, J.-C. Berthet, T. Cantat, P. Thuéry, N. Mézailles, P. Le Floch, et al., Organometallics 30 (2011) 2957.
[37] P.B. Iveson, C. Rivière, D. Guillaneux, M. Nierlich, P. Thuéry, M. Ephritikhine, et al., Chem. Commun. (2001) 1512.
[38] F.W. Lewis, L.M. Harwood, M.J. Hudson, A. Geist, V.N. Kozhevnikov, P. Distler, et al., Chem. Sci. 6 (2015) 4812.
[39] T. Mehdoui, J.-C. Berthet, P. Thuéry, L. Salmon, E. Rivière, M. Ephritikhine, Chem. Eur. J. 11 (2005) 6994.
[40] T. Cantat, C.R. Graves, B.L. Scott, J.L. Kiplinger, Angew. Chem. Int. Ed. 48 (2009) 3681.
[41] T. Cantat, B.L. Scott, D.E. Morris, J.L. Kiplinger, Inorg. Chem. 48 (2009) 2114.
[42] P.J. Fagan, J.M. Manriquez, T.J. Marks, C.S. Day, S.H. Vollmer, V.W. Day, Organometallics 1 (1982) 170.
[43] M. Ephritikhine, Angew. Chem. Int. Ed. 48 (2009) 4898.
[44] T. Arliguie, M. Blug, P. Le Floch, N. Mézailles, P. Thuéry, M. Ephritikhine, Organometallics 27 (2008) 4158.
[45] T. Arliguie, M. Doux, N. Mézailles, P. Thuéry, P. Le Floch, M. Ephritikhine, Inorg. Chem. 45 (2006) 9907.
[46] M. Doux, P. Thuéry, M. Blug, L. Ricard, P. Le Floch, T. Arliguie, et al., Organometallics 26 (2007) 5643.
[47] O.J. Cooper, D.P. Mills, J. McMaster, F. Tuna, E.J.L. McInnes, W. Lewis, et al., Chem. Eur. J. 19 (2013) 7071.
[48] D.P. Mills, F. Moro, J. McMaster, J. van Slageren, W. Lewis, A.J. Blake, et al., Nat. Chem. 3 (2011) 454.
[49] M.J. Sarsfield, M. Helliwell, D. Collison, Chem. Commun. (2002) 2264.
[50] M.J. Sarsfield, H. Steele, M. Helliwell, S.J. Teat, Dalton Trans. (2003) 3443.
[51] K.R. Johnson, M.A. Hannon, J.S. Ritch, P.G. Hayes, Dalton Trans. 41 (2012) 7873.
[52] M.M. Hänninen, M.T. Zamora, C.S. MacNeil, J.P. Knott, P.G. Hayes, Chem. Commun. 52 (2016) 586.
[53] J.P. Knott, M.M. Hänninen, J.M. Rautiainen, H.M. Tuononen, P.G. Hayes, J. Organomet. Chem. 845 (2017) 135.
[54] M.T. Zamora, K.R. Johnson, M.M. Hänninen, P.G. Hayes, Dalton Trans. 43 (2014) 10739.
[55] Dickie, T.K.K.; Hayes, P.G. Unpublished work, 2017.

[56]   C.A. Cruz, D.J.H. Emslie, L.E. Harrington, J.F. Britten, C.M. Robertson, Organometallics 26 (2007) 692.
[57]   C.A. Cruz, T. Chu, D.J.H. Emslie, H.A. Jenkins, L.E. Harrington, J.F. Britten, J. Organomet. Chem. 695 (2010) 2798.
[58]   C.A. Cruz, D.J.H. Emslie, L.E. Harrington, J.F. Britten, Organometallics 27 (2008) 15.
[59]   P.G. Hayes, W.E. Piers, R. McDonald, J. Am. Chem. Soc. 124 (2002) 2132.
[60]   M. Vogt, V. Pons, D.M. Heinekey, Organometallics 24 (2005) 1832.
[61]   C. Bonaccorsi, F. Santoro, S. Gischig, A. Mezzetti, Organometallics 25 (2006) 2002.
[62]   C.A. Cruz, D.J.H. Emslie, C.M. Robertson, L.E. Harrington, H.A. Jenkins, J.F. Britten, Organometallics 28 (2009) 1891.
[63]   N.R. Andreychuk, S. Ilango, B. Vidjayacoumar, D.J.H. Emslie, H.A. Jenkins, Organometallics 32 (2013) 1466.
[64]   B. Vidjayacoumar, S. Ilango, M.J. Ray, T. Chu, K.B. Kolpin, N.R. Andreychuk, et al., Dalton Trans. 41 (2012) 8175.
[65]   K.C. Jantunen, R.J. Batchelor, D.B. Leznoff, Organometallics 23 (2004) 2186.
[66]   K.C. Jantunen, F. Haftbaradaran, M.J. Katz, R.J. Batchelor, G. Schatte, D.B. Leznoff, Dalton Trans.  (2005) 3083.
[67]   J.-C. Tourneux, J.-C. Berthet, T. Cantat, P. Thuéry, N. Mézailles, M. Ephritikhine, J. Am. Chem. Soc. 133 (2011) 6162.
[68]   T. Cantat, T. Arliguie, A. Noël, P. Thuéry, M. Ephritikhine, P. Le Floch, et al., J. Am. Chem. Soc. 131 (2009) 963.
[69]   M. Ephritikhine, C. R. Chim. 16 (2013) 391.
[70]   J.-C. Tourneux, J.-C. Berthet, P. Thuéry, N. Mézailles, P. Le Floch, M. Ephritikhine, Dalton Trans. 39 (2010) 2494.
[71]   G. Ma, M.J. Ferguson, R. McDonald, R.G. Cavell, Inorg. Chem. 50 (2011) 6500.
[72]   O.J. Cooper, J. McMaster, W. Lewis, A.J. Blake, S.T. Liddle, Dalton Trans. 39 (2010) 5074.
[73]   O.J. Cooper, D.P. Mills, W. Lewis, A.J. Blake, S.T. Liddle, Dalton Trans. 43 (2014) 14275.
[74]   O.J. Cooper, D.P. Mills, J. McMaster, F. Moro, E.S. Davies, W. Lewis, et al., Angew. Chem. Int. Ed. 50 (2011) 2383.
[75]   M. Gregson, E. Lu, D.P. Mills, F. Tuna, E.J.L. McInnes, C. Hennig, et al., Nat. Commun. 8 (2017) 14137.
[76]   M. Gregson, E. Lu, F. Tuna, E.J.L. McInnes, C. Hennig, A.C. Scheinost, et al., Chem. Sci. 7 (2016) 3286.
[77]   M. Gregson, A.J. Wooles, O.J. Cooper, S.T. Liddle, Comments Inorg. Chem. 35 (2015) 262.
[78]   Liddle, S.T.; Mills, D.P.; Wooles, A.J. Organometallic Chemistry: Volume 36; The Royal Society of Chemistry: 2010; Vol. 36, 29.
[79]   E. Lu, O.J. Cooper, J. McMaster, F. Tuna, E.J.L. McInnes, W. Lewis, et al., Angew. Chem. Int. Ed. 53 (2014) 6696.
[80]   E. Lu, O.J. Cooper, F. Tuna, A.J. Wooles, N. Kaltsoyannis, S.T. Liddle, Chem. Eur. J. 22 (2016) 11559.
[81]   E. Lu, W. Lewis, A.J. Blake, S.T. Liddle, Angew. Chem. Int. Ed. 53 (2014) 9356.
[82]   E. Lu, F. Tuna, W. Lewis, N. Kaltsoyannis, S.T. Liddle, Chem. Eur. J. 22 (2016) 11554.
[83]   D.P. Mills, O.J. Cooper, F. Tuna, E.J.L. McInnes, E.S. Davies, J. McMaster, et al., J. Am. Chem. Soc. 134 (2012) 10047.
[84]   A. Kasani, R.P. Kamalesh Babu, R. McDonald, R.G. Cavell, Angew. Chem. Int. Ed. 38 (1999) 1483.
[85]   C.M. Ong, D.W. Stephan, J. Am. Chem. Soc. 121 (1999) 2939.
[86]   R.E. Cramer, R.B. Maynard, J.C. Paw, J.W. Gilje, J. Am. Chem. Soc. 103 (1981) 3589.
[87]   W. Ren, X. Deng, G. Zi, D.-C. Fang, Dalton Trans. 40 (2011) 9662.
[88]   R.E. Da Re, K.C. Jantunen, J.T. Golden, J.L. Kiplinger, D.E. Morris, J. Am. Chem. Soc. 127 (2005) 682.
[89]   F. Guérin, D.H. McConville, J.J. Vittal, Organometallics 14 (1995) 3154.
[90]   F. Guérin, D.H. McConville, J.J. Vittal, Organometallics 15 (1996) 5586.
[91]   F. Guérin, D.H. McConville, J.J. Vittal, G.A.P. Yap, Organometallics 17 (1998) 5172.
[92]   C.A. Cruz, D.J.H. Emslie, H.A. Jenkins, J.F. Britten, Dalton Trans. 39 (2010) 6626.
[93]   A.F. England, C.J. Burns, S.L. Buchwald, Organometallics 13 (1994) 3491.
[94]   S. Duhovic, S. Khan, P.L. Diaconescu, Chem. Commun. 46 (2010) 3390.
[95]   D.J. Wilson, A. Sebastian, F.G.N. Cloke, A.G. Avent, P.B. Hitchcock, Inorg. Chim. Acta 345 (2003) 89.
[96]   I. Korobkov, S. Gorelsky, S. Gambarotta, J. Am. Chem. Soc. 131 (2009) 10406.
[97]   O.R. Luca, R.H. Crabtree, Chem. Soc. Rev. 42 (2013) 1440.
[98]   V. Lyaskovskyy, B. de Bruin, ACS Catal. 2 (2012) 270.
[99]   S.N. Brown, Inorg. Chem. 51 (2012) 1251.
[100]   J.J. Kiernicki, R.F. Higgins, S.J. Kraft, M. Zeller, M.P. Shores, S.C. Bart, Inorg. Chem. 55 (2016) 11854.
[101]   J.J. Kiernicki, B.S. Newell, E.M. Matson, N.H. Anderson, P.E. Fanwick, M.P. Shores, et al., Inorg. Chem. 53 (2014) 3730.
[102]   B.L. Small, M. Brookhart, A.M.A. Bennett, J. Am. Chem. Soc. 120 (1998) 4049.
[103]   G.J.P. Britovsek, V.C. Gibson, S.J. McTavish, A.G. Solan, A.J.P. White, D.J. Williams, et al., Chem. Commun.  (1998) 849.
[104]   B.L. Small, Acc. Chem. Res. 48 (2015) 2599.
[105]   V.C. Gibson, C. Redshaw, G.A. Solan, Chem. Rev. 107 (2007) 1745.
[106]   B. de Bruin, E. Bill, E. Bothe, T. Weyhermüller, K. Wieghardt, Inorg. Chem. 39 (2000) 2936.
[107]   P.J. Chirik, K. Wieghardt, Science 327 (2010) 794.
[108]   J.M. Hoyt, V.A. Schmidt, A.M. Tondreau, P.J. Chirik, Science 349 (2015) 960.
[109]   D.P. Cladis, J.J. Kiernicki, P.E. Fanwick, S.C. Bart, Chem. Commun. 49 (2013) 4169.
[110]   J.J. Kiernicki, M.G. Ferrier, J.S. Lezama Pacheco, H.S. La Pierre, B.W. Stein, M. Zeller, et al., J. Am. Chem. Soc. 138 (2016) 13941.
[111]   J.J. Kiernicki, D.P. Cladis, P.E. Fanwick, M. Zeller, S.C. Bart, J. Am. Chem. Soc. 137 (2015) 11115.
[112]   N.H. Anderson, S.O. Odoh, U.J. Williams, A.J. Lewis, G.L. Wagner, J. Lezama Pacheco, et al., J. Am. Chem. Soc. 137 (2015) 4690.
[113]   N.H. Anderson, S.O. Odoh, Y. Yao, U.J. Williams, B.A. Schaefer, J.J. Kiernicki, et al., Nat. Chem. 6 (2014) 919.

[114]   E.P. Ivakhnenko, A.G. Starikov, V.I. Minkin, K.A. Lyssenko, M.Y. Antipin, V.I. Simakov, et al., Inorg. Chem. 50 (2011) 7022.

[115]   L.G. Ranis, K. Werellapatha, N.J. Pietrini, B.A. Bunker, S.N. Brown, Inorg. Chem. 53 (2014) 10203.

[116]   S.A. Pattenaude, C.S. Kuehner, W.L. Dorfner, E.J. Schelter, P.E. Fanwick, S.C. Bart, Inorg. Chem. 54 (2015) 6520.

[117]   G. Szigethy, A.F. Heyduk, Dalton Trans. 41 (2012) 8144.

[118]   P.L. Arnold, Z.R. Turner, Nat. Rev. Chem. 1 (2017) 0002.

[119]   B.D. Stubbert, C.L. Stern, T.J. Marks, Organometallics 22 (2003) 4836.

[120]   C.J. Weiss, T.J. Marks, Dalton Trans. 39 (2010) 6576.

[121]   R.D. Gillespie, R.L. Burwell, T.J. Marks, Langmuir 6 (1990) 1465.

[122]   C.E. Hayes, R.H. Platel, L.L. Schafer, D.B. Leznoff, Organometallics 31 (2012) 6732.

[123]   C.E. Hayes, Y. Sarazin, M.J. Katz, J.-F. Carpentier, D.B. Leznoff, Organometallics 32 (2013) 1183.

[124]   C.E. Hayes, D.B. Leznoff, Organometallics 29 (2010) 767.